Research Square

Preprints are preliminary reports that have not undergone peer review.
They should not be considered conclusive, used to inform clinical practice,
or referenced by the media as validated information.

Strengthening microbial carbon and phosphorus co-limitation during subtropical forest restoration

Jinlei Chen

570615001@qq.com

guang xi ke xue yuan: Guangxi Academy of Sciences https://orcid.org/0009-0003-9086-7731

Xi Fang

Zhiwei Cao

Xiaoye Zhu

Huiying Lin

Hans Lambers

Xiaoguo Zhou

Junmo Xu

Yongjie Huang

Dongjing Sun

Yuanguang Wen

Enqing Hou

https://orcid.org/0000-0003-4864-2347

Research Article

Keywords: soil ecoenzymatic stoichiometry, microbial carbon-phosphorus co-limitation, vegetation restoration, subtropical forest, vector analysis

Posted Date: November 18th, 2026

DOI: https://doi.org/10.21203/rs.3.rs-11516756/v1

License: This work is licensed under a Creative Commons Attribution 4.0 International License.
Read Full License

Strengthening microbial carbon and phosphorus co-limitation during subtropical forest restoration

Jinlei Chen [a], Xi Fang [b *], Zhiwei Cao [c], Xiaoye Zhu [d], Huiying Lin [e], Hans Lambers [f], Xiaoguo Zhou [a], Junmo Xu [a], Yongjie Huang [a], Dongjing Sun [a], Yuanguang Wen [a], Enqing Hou [e *]

[a] Institute of Eco-Environment Research, Guangxi Academy of Sciences, Nanning 530007, Guangxi, China

[b] School of Ecology and Environment, Central South University of Forestry and Technology, Changsha 410004, China

[c] Department of Atmospheric and Oceanic Sciences & Institute of Atmospheric Sciences, Fudan University, Shanghai 200438, China

[d] Hunan Geospatial Information Engineering and Technology Research Center, Hunan Province Third Surveying and Mapping Institute, Changsha 410011, China

[e] Guangdong Provincial Key Laboratory of Applied Botany & Key Laboratory of National Forestry and Grassland Administration on Plant Conservation and Utilization in Southern China, South China Botanical Garden, Chinese Academy of Sciences, Guangzhou 510650, China

[f] School of Biological Sciences, University of Western Australia, Perth 6009, Australia

* Corresponding author: Enqing Hou

E-mail address: houeq@scbg.ac.cn

* Co-corresponding author: Xi Fang

E-mail address: fangxizhang@sina.com

Abstract:

Aims: Subtropical forest restoration is expected to alter soil microbial nutrient limitation, yet the successional trajectory and underlying drivers remain poorly understood. In this study, we investigated how microbial carbon (C) and phosphorus (P) limitation shift along a typical restoration chronosequence and identified the key biotic and abiotic factors influencing these shifts.

Methods: We selected a restoration chronosequence in subtropical China, spanning early *Pinus massoniana* plantation (PM), mid-stage *P. massoniana–Lithocarpus glaber* mixed forest (PL) and *Choerospondias axillaris* deciduous broadleaf forest (CA), and late-stage *L. glaber* evergreen broadleaf forest (LG). Soil enzyme activities, litter properties, soil physicochemical traits, and microbial biomass were measured. Microbial C and P limitation were quantified using vector analysis and threshold elemental ratio modeling, with Random Forest and PLS-PM used to identify key drivers.

Results: β-D-glucosidase (BG), β-N-acetylglucosaminidase (NAG), and acid phosphatase (ACP) exhibited a unimodal pattern peaking at CA, while cellobiohydrolase (CBH) declined continuously. Microbial C-P co-limitation intensified along succession, with LG exhibiting the highest vector length (0.79) and angle (80.04°). Litter nitrogen and litter C:N ratio emerged as primary predictors of C limitation, while microbial biomass N:P and C:N predicted P limitation. Soil properties exerted the strongest positive effect on C limitation but the strongest negative effect on P limitation.

Conclusions: Vegetation restoration was accompanied by a shift from weak C and moderate P limitation in early *P. massoniana* forests to severe C-P co-limitation in late broadleaved

forests, a transition likely influenced by increased litter recalcitrance, stoichiometric imbalances, and plant-microbe competition. Therefore, managing litter quality and nutrient stoichiometry may help alleviate microbial co-limitation and sustain soil carbon sequestration.

Keywords: soil ecoenzymatic stoichiometry; microbial carbon-phosphorus co-limitation; vegetation restoration; subtropical forest; vector analysis

1 Introduction

Soil microbes are key factors affecting soil carbon (C) cycling and nutrient cycling (Hu et al., 2016; Cui et al., 2021). Meanwhile, their growth is also affected by the availability of C and nutrients (mainly nitrogen (N) and phosphorus (P)), and an imbalance in their availability can lead to microbial resource limitation (Traoré et al., 2016). Comparison with that in plants, the metabolic limitation of soil microbes remains less studied across sites, for example along forest succession gradients, despite its decisive role in modulating soil functions and processes (Turner et al., 2024; Cui et al., 2025**)**. Vegetation restoration projects across the world have profoundly altered plant community composition, litter input characteristics, and soil physicochemical properties, thereby reshaping soil nutrient stoichiometric balance (Burke et al., 2011; Sinsabaugh & Follstad Shah, 2011; Chen et al., 2020). Therefore, clarifying whether and how microbial nutrient limitation would shift during vegetation restoration is critical for predicting the restoration of key soil functions such as carbon sequestration and nutrient cycling.

Ecoenzymatic stoichiometry provides a robust, and mechanistic framework for quantitatively evaluating microbial resource limitation by linking extracellular enzyme activity to microbial metabolic resource demand (Sinsabaugh et al., 2008). Soil microorganisms secrete specific extracellular enzymes that depolymerize complex organic compounds and acquire available energy and nutrients for growth and metabolism (Sterner & Elser 2002; Duan et al. 2018). Typically, β-D-glucosidase (BG) and cellobiohydrolase (CBH) are representative C-acquiring enzymes responsible for cellulose degradation; β-N-acetylglucosaminidase (NAG) dominates organic N mineralization; and acid phosphatase

(ACP) is the key P-acquiring enzyme that hydrolyzes organic P substrates (Sinsabaugh et al., 2009). The relative activity ratios of these enzymes can effectively reflect microbial resource limitation status: microbes tend to invest more resources that synthesizing specific nutrient-acquiring enzymes that alleviate corresponding resource shortages under nutrient-deficient conditions (Allison et al., 2007; Sinsabaugh & Follstad Shah, 2012; Gong et al., 2025). Recent studies suggest that traditional qualitative enzymatic inference has limitations in accuracy and comparability, and standalone enzymatic stoichiometry indicators may produce biased interpretation under complex environmental conditions (Mori, 2024).

To overcome the defects of qualitative judgment, vector analysis and threshold elemental ratio (TER) modeling are widely recognized as effective tools to quantify the intensity and direction of microbial nutrient limitation (Sinsabaugh et al., 2009; Moorhead et al., 2016). The TER model defines the critical elemental ratio threshold for the transition between microbial nutrient and carbon limitation (Sinsabaugh et al., 2009), while enzymatic vector analysis integrates the relative activities of C-, N-, and P-acquiring enzymes into a two-dimensional coordinate system, where vector length indicates the degree of microbial C limitation and vector angle differentiates N versus P limitation intensity. Combined application of the two methods achieves quantitative and reliable assessment of microbial resource limitation (Cui et al., 2024). Studies have revealed distinct microbial limitation patterns across ecosystems: arid ecosystems are generally constrained by C-P co-limitation (Cui et al., 2019; Xiao et al., 2020), while tropical old-growth forests are predominantly limited by P (Waring et al., 2014). Recent meta-analyses further confirmed that forest stand transformation alters extracellular enzyme activities and relieves microbial C limitation to a

certain extent, yet C-P co-limitation remains prevalent in forest ecosystems (Fan et al., 2025). However, how and why microbial nutrient limitation would shift during vegetation restoration remains unclear.

Subtropical China is an ideal region for exploring microbial nutrient limitation during forest restoration. The highly weathered iron- and aluminum-rich acidic red soils in this region are chronically P-deficient, providing an inherent P-limited soil environment for soil microbial growth (Huang et al., 2013; Hou et al., 2018). Over the past decades, large-scale vegetation restoration projects, including the Natural Forest Protection Program and the Grain-to-Green Program, have promoted the progressive succession of degraded subtropical forests, forming a complete restoration chronosequence from early coniferous plantations to late-evergreen broadleaved forests (Chen et al., 2020). While previous studies on forest succession usually assumed that soil microbial nutrient limitation would be alleviated and microbial metabolic status would increase during forest succession (Yang et al., 2024; Gao et al., 2024), there is still a lack of empirical tests. Studies show microbial nutrient dynamics along forest restoration gradients in this region and confirmed the universal existence of microbial C and P limitation (Wan et al., 2025; Zhang et al., 2022; Pang et al., 2025). However, most of these studies have explored how soil nutrient availability or litter chemistry would affect microbial nutrient limitation during vegetation restoration (Zhang et al., 2022; Pang et al., 2025), but ignored the potential synergistic influences of litter structural recalcitrance, microbial biomass stoichiometric imbalance, and plant-microbe nutrient competition, and thus provide incomplete insights into the drivers of soil microbial nutrient limitation during forest succession. To fill this gap, we selected four typical forests

along a forest restoration gradient in subtropical China. We comprehensively measured forest floor litter properties, soil physicochemical characteristics, microbial biomass stoichiometry, and the activities of four key C/N/P-acquiring enzymes (BG, CBH, NAG, ACP). By integrating vector analysis, TER modeling, random forest, and partial least squares path modeling (PLS-PM), we quantitatively characterized microbial nutrient limitation along the restoration chronosequence and identified the key drivers.

We proposed two hypotheses to test: (*H1*) soil microbial C and P limitation would emerge due to different factors, specifically microbial C limitation emerges due to low quantity and quality of C input, while microbial P limitation develops due to the low availability of P relative to other soil elements (mainly of C and N) (Cui et al., 2019; Hou et al., 2018; Cui et al., 2022); (*H2*) microbial metabolic limitation would shift from C limitation to C-P co-limitation during vegetation restoration, because soil organic C availability is typically low at the early stage but C accumulates with the restoration of vegetation, while the opposite is usually true for soil P availability (Zhang et al., 2022; Wan et al., 2025). Testing these hypotheses can offer theoretical support to targeted forest management strategies to alleviate microbial nutrient co-limitation and thus promote soil C sequestration in subtropical forests.

2 Materials and methods

2.1 Study site and sampling

This study was conducted in Dashanchong Forest Park (28°23′58″-28°24′58″ N, 113°17′46″-113°19′8″ E), Changsha County, Hunan Province, China. The climate is humid,

with a mean annual temperature of 17.3℃ and mean annual precipitation of 1416 mm, approximately 70% of which falls between April and August, conditions that favor rapid forest secondary succession. The terrain consists mainly of low hills, with elevations ranging from 55 to 217 m. Soils are classified as Alliti-Udic Ferrosols (FAO system), developed from slate and shale parent materials. These soils are characterized by a high clay content, strong acidity, good drainage, and inherent P deficiency resulting from intensive iron-aluminum oxide sorption, typical properties of highly-weathered subtropical red soils. The zonal vegetation is evergreen broadleaved forest. The study area includes a complete sequence of secondary forests and plantations dominated by *Pinus massonian*, *Lithocarpus glaber* , *Choerospondias axillaris*, and *Cyclobalanopsis glauca*, providing ideal conditions for exploring vegetation succession and associated soil biogeochemical dynamics.

We employed the widely used space-for-time substitution approach to investigate successional dynamics of microbial nutrient limitation. Field sampling was carried out in June 2019. Strict site selection criteria were applied to ensure comparability and regional representativeness: all selected stands share consistent geographical backgrounds, similar micro-topography (elevation, slope, and aspect), identical soil parent material, and uniform regional climate, differing primarily in restoration stage and community structure. Four typical forest communities representing early, middle, transitional, and late secondary restoration stages were selected to form a complete subtropical forest succession gradient, covering the dominant vegetation transition from coniferous plantation to mixed forest and finally to zonal evergreen broadleaved forest:

(1) *P. massoniana* plantation (early restoration stage, PM). This stand originated from

aerial seeding of *P. massoniana* during 1983-1985 after the clear-cutting of primary evergreen broadleaved forests, with no history of fertilization or intensive management. Canopy closure occurred 10-15 years after afforestation, and the stand has since been protected under near-natural management. At a current age of 30-35 years, it represents the early successional coniferous forest stage widely distributed in degraded subtropical red soil hilly areas.

(2) *P. massoniana-L. glaber* mixed coniferous-broadleaved forest (mid-restoration stage, PL). This stand developed via natural secondary succession after the clear-cutting of native evergreen broadleaved forest in the early 1970s, with a current age of 45-50 years. Stand basal area comprises 50% *P. massoniana*, 17% *L. glaber*, and 33% other broadleaved species. The community has abundant understory seedlings and saplings with moderate stand density, representing the typical transition from pure coniferous to mixed forest in subtropical restoration.

(3) *C. axillaris* deciduous broadleaved forest (transitional restoration stage, CA). This community developed from natural secondary succession on abandoned lands after firewood harvesting was prohibited in the late 1950s, with a current age of 60-70 years. Stand basal area is dominated by 58% *C. axillaris*, accompanied by 18% *Quercus fabri* and 24% other companion species. Large-diameter trees are primarily *C. axillaris*, while most other species occur in the understory, representing the deciduous broadleaved transitional stage in subtropical forest succession.

(4) *L. glaber* evergreen broadleaved forest (late-restoration stage, LG). This well-preserved native evergreen broadleaved forest has experienced negligible anthropogenic and

184 livestock disturbance, with a stand age of 80-90 years. The community has complex species
185 composition, stable stand structure, and mature canopy stratification, representing the climax
186 zonal vegetation of mid-subtropical hilly red soil regions.

187 For each forest stage, we established four independent 30 m×30 m sampling plots. To
188 ensure spatial independence and avoid pseudoreplicated locations, the distance between any
189 two plots within the same successional stage exceeded 1000 m (Fig. 1). Each plot was further
190 divided into nine 10 m × 10 m subplots for detailed community structure and vegetation
191 surveys. Basic stand characteristics for all plots are summarized in Table 1.

192 Litter, soil, and fine root samples were collected in July 2020. Within each 30 m × 30
193 m plot, three sampling points were evenly arranged along the plot diagonal. At each point, a
194 1 m × 1 m quadrat was randomly placed, and all intact aboveground litter on the soil surface
195 was collected. Litter samples from the three quadrats within a plot were thoroughly mixed
196 and pooled into one composite sample per plot, yielding 16 litter composite samples (4
197 plots × 4 stages). Samples were placed in clean cloth bags and transported to the laboratory
198 promptly. After removing residual impurities, the samples were oven-dried at 75°C to a
199 constant weight, ground into fine powder with a mechanical grinder, and sieved through a
200 0.25-mm mesh for determination of litter chemical properties.

201 Immediately following litter collection, mineral soil cores were taken from the same
202 three diagonal sampling points at a depth of 0-15 cm. The three cores from each plot were
203 fully homogenized to form a single composite sample, giving 16 soil samples in total (4 plots
204 per stage × 4 stages). All soil samples were temporarily stored in ice-cooled insulated boxes,
205 rapidly transported to the laboratory, and kept at 4°C for subsequent processing. Each

206 composite sample was divided into two portions: one portion of fresh soil was sieved through
207 a 2-mm mesh and used immediately for analysis of extracellular enzyme activities and
208 microbial biomass; the remaining portion was air-dried at room temperature and sequentially
209 sieved through different mesh sizes (2 mm for soil particle analysis, 1-mm for pH
210 measurement, and 0.25 mm for soil nutrient quantification).

211 Fine root biomass was determined following the standardized method of Liu et al.
212 (2014). In each plot, five sampling points were arranged in a five-point pattern. After
213 removing the surface humus and litter layer, soil cores were collected from the 0-15 cm
214 mineral soil layer using an auger (10 cm inner diameter, 15 cm height). All cores were sealed
215 in plastic bags and stored at 4°C. Fine root sorting and weighing were completed within one
216 month after field sampling. Each core was fully soaked in tap water and rinsed through a
217 0.25 mm sieve until fine roots were completely separated from soil particles. Roots with a
218 diameter ≤ 2 mm were selected, oven-dried at 75°C to constant mass, and weighed to
219 calculate fine root biomass.

220 **2.2 Litter, fine roots, and soil physicochemical and microbial properties**

221 Organic C concentrations in litter, fine root, and soil samples were determined using the
222 potassium dichromate–sulfuric acid ($K_2Cr_2O_7$-H_2SO_4) digestion method (Deng et al., 2013).
223 Total nitrogen (TN) was measured via the Kjeldahl digestion procedure (Deng et al., 2013).
224 Total phosphorus (TP) was determined using the molybdenum-antimony colorimetric
225 method after acid digestion with HCl-HNO_3 (ISO 54321:2020; Ivanov et al., 2012). Plant-
226 available soil phosphorus (AP) was determined by double-acid extraction with hydrochloric
227 and sulfuric acids followed by colorimetric analysis (Mehlich, 1953). Soil pH was measured

in a 1:2.5 (w/v) soil-to-water suspension using a pH meter (FE20, Mettler Toledo, Switzerland). Soil particle size distribution was analyzed using a laser particle size analyzer (Mastersizer 3000, Malvern, UK). Soil ammonium nitrogen (NH_4^+-N) and nitrate nitrogen (NO_3^--N) were extracted with 2 M K_2SO_4 and quantified with a continuous flow analyzer (Skalar Analytical BV, Breda, the Netherlands). Total iron (Fe) and total aluminum (Al) concentrations were determined by inductively coupled plasma atomic emission spectrometry (Optima 8300, PerkinElmer, Waltham, USA).

Soil microbial biomass C (MBC), N (MBN), and P (MBP) were determined using the chloroform fumigation-extraction method. Concentrations of MBC and MBN in fumigated and non-fumigated extracts were measured with a total organic C analyzer (TOC-1020A, Shimadzu, Kyoto, Japan), and MBP was determined by the molybdenum-antimony colorimetric method (Wu et al., 2000). Conversion factors for MBC, MBN, and MBP were 0.45, 0.54, and 0.40, respectively (Joergensen & Mueller, 1996).

2.3 Assays of enzymatic activity

Soil extracellular enzyme activities were measured using a 96-well microplate fluorometric assay following standard fluorescence protocols (Saiya-Cork et al. 2002). Four key enzymes associated with soil C, N, and P cycling were measured: two C-acquiring enzymes (β-1,4-glucosidase, BG; cellobiohydrolase, CBH), one N-acquisition enzyme (β-1,4-N-acetylglucosaminidase, NAG), and one P-acquisition enzyme (acid phosphatase, ACP). Briefly, 1 g of fresh sieved soil was mixed with 125 mL of 50 mM sodium acetate buffer (pH 5.0) and continuously stirred to obtain a uniform soil slurry. Each 96-well microplate was divided into blank, standard, negative control, soil control, quench standard,

and sample wells, with four analytical replicates for each treatment. Blank wells contained only sodium acetate buffer; standard wells contained buffer plus fluorescent standard solution; negative control wells contained buffer plus enzyme substrate solution; soil control wells contained soil slurry plus buffer; quench correction wells contained soil slurry plus standard solution; and sample wells contained soil slurry plus fluorescent substrate. All microplates were incubated at 25°C for 4 h in the dark. A microplate fluorometer was used to determine fluorescence at 365 nm excitation and 450 nm emission (German et al., 2011).

2.4 Vector analysis of enzymatic activities

Microbial metabolic limitation was quantitatively evaluated via enzymatic vector analysis and threshold elemental ratio (TER) modeling. We calculated vector lengths and vector angles based on non-transformed extracellular enzyme activity data. Vector length indicates the degree of C limitation, while vector angle distinguishes N versus P limitation intensity. Calculations followed Moorhead et al. (2016):

$$Vector\ \text{Length} = \sqrt{(x^2 + y^2)} \quad (1)$$

$$Vector\ Angle(°) = DEGREES(ATAN2(x, y)) \quad (2)$$

where x = (βG + CBH)/(βG + CBH + AP), and y = (βG + CBH)/ (βG + CBH + NAG). Longer vector lengths indicate greater microbial C limitation, and greater vector angles indicate stronger P limitation relative to N limitation. However, the classical 45° threshold (Moorhead et al., 2016) has been challenged for overestimating P limitation in subtropical P−deficient soils. Thus, we adopted updated criteria: vector length > 0.61 indicates C limitation, and vector angle > 55° indicates significant P limitation (Cui et al., 2024; Mori, 2020).

We combined this with the threshold element ratio (TER) model to clarify the distinction between microbial C and nutrient limitation. TER values for C:N and C:P were defined as the element ratio corresponding to balanced microbial growth, calculated following Sinsabaugh et al. (2009):

$$TER_{C:N} = \left(\frac{BG+CBH}{NAG}\right) \times \frac{B_{C:N}}{n_0} \quad (3)$$

$$TER_{C:P} = \left(\frac{BG+CBH}{ACP}\right) \times \frac{B_{C:P}}{p_0} \quad (4)$$

where $TER_{C:N}$ and $TER_{C:P}$ are the threshold elemental ratios for C:N and C:P, respectively; $B_{C:N}$ and $B_{C:P}$ indicate microbial biomass C:N and C:P ratio; n_0 and p_0 are normalization constants for N and P. n_0 represents the intercept of the log‑transformed regression between log(BG+CBH) and log(NAG), and p_0 represents the intercept of the regression between log(BG+CBH) and log(AP) (Wang et al., 2026).

2.5 Statistical analyses

All statistical analyses were conducted using SPSS 24.0 (IBM SPSS Inc. Chicago, USA) and R software (v 4.5.1). Data were tested for normality and homogeneity of variance using Shapiro-Wilk and Levene's test, respectively. Data that did not conform to normal distribution were log-transformed to meet parametric test assumptions. One-way analysis of variance (ANOVA), followed by least significant difference (LSD) post-hoc test was conducted to assess differences in litter, roots, soil, microbial, and enzymatic properties among the four restoration stages.

Random forest analysis *(R package "random Forest*") was used to quantitatively rank the relative importance of driving factors affecting microbial C and P limitations. Partial least squares path modeling (PLS-PM, R package "plspm") was constructed to unravel the

direct and indirect pathways by which litter properties, fine root traits, soil physicochemical characteristics, and microbial biomass stoichiometry impact microbial metabolic limitation. To minimize multicollinearity, variables with variance inflation factor (VIF) > 10 were excluded from the final model. The final pathway framework was constructed based on the dominant predictive factors from random forest analysis and theoretical ecological mechanisms.

3 Results

3.1 Variation in soil physicochemical properties along a vegetation restoration chronosequence

Vegetation restoration significantly altered soil physical structure and physicochemical characteristics across the successional chronosequence (Table 2). Soil bulk density decreased significantly with forest restoration ($p < 0.05$), with the lowest value observed in the transitional deciduous broadleaved stage (CA, 1.1 g cm^{-3}). Soil clay content increased significantly, while sand and silt fractions decreased significantly during succession ($p < 0.05$). The proportional ranges of sand, silt, and clay across all stands were 8.4-10.8%, 57.7-68.1%, and 21.1-33.8%, respectively. Soil pH was consistently acidic throughout restoration, ranging from 4.1 (mid-stage mixed forest, PL) to 4.3 (CA). Soil nutrient indicators differed significantly among four restoration stages ($p < 0.05$). Specifically, SOC, TN, TP, DOC, NO_3^--N, and AP concentrations were all significantly higher in the CA stage than in PM, PL, and LG. From PM to PL, SOC, TN, and NO_3^--N concentrations decreased significantly ($p < 0.05$), while TP and DOC concentrations increased ($p < 0.05$). From CA to LG, nearly all

soil nutrient variables (except NH_4^+-N concentration) decreased significantly ($p < 0.05$). NH_4^+-N concentration peaked in PM (20.1 mg kg^{-1}) and was lowest in LG (16.8 mg kg^{-1}), though differences were not statistically significant. Soil nutrient stoichiometry also showed significant successional differentiation ($p < 0.05$): the soil C:N ratio was highest in CA (15.6) and lowest in PM (11.0); the C:P ratio was highest in CA (102.2) and lowest in LG (77.0); the N:P ratio was highest in PM (7.6) and lowest in LG (5.4) (Table 2).

3.2 Dynamics of soil microbial biomass and stoichiometric characteristics

Soil MBC, MBN, and MBP concentrations varied significantly along the vegetation restoration chronosequence, exhibiting a consistent unimodal successional pattern (Table 3, $p < 0.05$). All microbial biomass components reached their maximum values at the CA stage, with MBC of 794 ± 25 mg kg^{-1}, MBN of 95 ± 1.8 mg kg^{-1}, and MBP of 23.7 ± 1.0 mg kg^{-1}. We observed the lowest values in the early-stage PM plantation, with MBC, MBN, and MBP concentrations of 525.1 ± 25.4, 59.7 ± 2.4, and 10.4 ± 0.5 mg kg^{-1}, respectively. Vegetation restoration also significantly reshaped microbial biomass stoichiometric ratios ($p < 0.05$). The MBC:N ratio was lowest in the PL stage (8.2 ± 0.4) and increased gradually in later stages. Both MBC:P and MBN:P ratios attained their minimum values in CA (33.6 ± 1.5 and 4.0 ± 0.2, respectively), significantly lower than in the other three stages ($p < 0.05$), indicating a more balanced microbial nutrient status in the transitional deciduous broadleaved forest.

3.3 Variation in soil extracellular enzyme activities

The activities of four key C-, N-, and P-acquiring extracellular enzymes and their stoichiometric ratios differed significantly across vegetation restoration stages (Fig. S1, Fig.

2, $p < 0.05$). The C-acquiring enzyme BG, N-acquiring enzyme NAG, and P-acquiring enzyme ACP all showed significantly higher activities in the CA stage than in the other three stands ($p < 0.05$), with peak values of 117.2 ± 4.7 nmol g^{-1} h^{-1} (BG), 48.9 ± 2.2 nmol g^{-1} h^{-1} (NAG), and 651.6 ± 30.0 nmol g^{-1} h^{-1} (ACP). In contrast, CBH activity exhibited a continuous decreasing trend along the restoration gradient ($p < 0.05$). The early-stage PM plantation had the highest CBH activity (10.1 ± 1.2 nmol g^{-1} h^{-1}), while no significant difference was detected between PL and CA.

Correlation analysis revealed divergent correlation patterns between environmental variables and enzyme activities (Table S3, Fig. 3). BG activity was strongly positively correlated with soil TP, DOC, and MBC concentrations ($r = 0.89$, 0.84, and 0.96, respectively, $p < 0.01$). CBH activity was positively correlated with soil Fe concentration and LC:N ($r =$ 0.90 and 0.76, respectively, $p < 0.01$) but negatively correlated with LTN ($r = -0.78$, $p <$ 0.01). NAG activity was positively correlated with FRN and soil NO_3^--N concentration ($r =$ 0.70 and 0.72, respectively, $p < 0.01$) but negatively correlated with Lsc concentration ($r =$ -0.87, $p < 0.01$). ACP activity was positively correlated with MBC and LTN concentrations ($r = 0.79$ and 0.68, $p < 0.01$), and negatively correlated with MBC:P ($r = -0.82$, $p < 0.01$).

3.4 Successional dynamics of microbial resource limitations

Enzymatic stoichiometry-based vector analysis indicated significant shifts in microbial resource limitation patterns during vegetation restoration (Fig. 4a). All sampling points fell to the left of the 55° threshold line, indicating that microbial metabolism was universally constrained by P limitation, rather than N limitation across all restoration stages. Both vector length and vector angle differed significantly among successional stages, with clear

intensification of microbial co-limitation in late-successional forest (Fig. 4b, c). The late-stage LG forest showed the greatest vector length (0.79) and vector angle (80.04°), representing the most severe microbial C-P co-limitations. In contrast, the early-stage PM plantation had the lowest vector length (0.63), and the transitional CA stage had the minimum vector angle (77.38°). Vector length was positively but non-significantly correlated with vector angle across the restoration gradient (Fig. 4d). TER modeling further verified successional changes in microbial limitation status. $TER_{C:N}$ increased significantly with vegetation restoration ($p < 0.05$), while $TER_{C:P}$ showed a slight but non-significant decreasing trend from early to late succession (Fig. 4e, f).

3.5 Dominant drivers of microbial resource limitations

Random forest analysis identified key predictive factors affecting microbial C and P limitation (Fig. 5a, b). Microbial C limitation (vector length) was primarily affected by the MBN:P ratio, which contributed the greatest increase in mean squared error (MSE), followed by MBC, LTN, LC:N and MBP concentrations. For microbial P limitation (vector angle), MBC:N was the dominant factor, followed by LN:P, LTN, soil C:P, and LC:P.

PLS-PM further clarified the direct and indirect pathways of multi-dimensional environmental factors affecting microbial resource limitations (Fig. 6). Soil properties exerted the strongest positive total effect on microbial C limitation (total effect = 0.91, Fig. 6 a, b) and the strongest negative total effect on microbial P limitation (total effect = -0.87, Fig. 6 c, d). Litter properties showed a significant positive direct effect on P limitation ($p < 0.05$) and a weak positive effect on C limitation. Fine root properties significantly promoted C limitation and alleviated P limitation ($p < 0.05$). Microbial biomass and stoichiometric

properties significantly enhanced microbial C limitation ($p < 0.05$) but had a negligible negative influence on P limitation.

4 Discussions

4.1 Factors affecting soil extracellular enzyme activities

Soil extracellular enzyme activities (EEAs) are crucial indicators of microbial metabolic investment, catalyzing the depolymerization of soil organic matter and affecting biogeochemical cycling of C, N, and P (Lozano *et al*., 2014; Raiesi, 2012; Zhao *et al*., 2023). Our study revealed that vegetation restoration substantially reshaped soil EEA patterns across the subtropical forest chronosequence. Specifically, BG, NAG, and ACP exhibited a unimodal trend, peaking in CA and declining in LG. In contrast, CBH decreased monotonically from PM to LG (Fig. 2). These heterogeneous EEA dynamics partially support our first hypothesis, which posits that microbial C and P limitations associated with distinct factors: C limitation is primarily associated with the quantity and quality of C inputs, whereas P limitation arises from the loid availability of P relative to other elements. Yet, enzyme activities do not simply increase with vegetation recovery but followed context-dependent successional trajectories, reflecting the divergent response pathways of different nutrient-acquiring enzymes.

The increases in BG, NAG, and ACP activities from PM to CA were primarily attributable to enhanced substrate availability and microbial metabolic activity. Our results show that SOC, TP, AP, DOC, and microbial biomass all peaked in CA (Tables 2 and 3). Abundant labile substrates and proliferating microbial communities jointly stimulated

402 microbial extracellular enzyme production to meet rapid growth and nutritional demands
403 (Chen et al., 2018). However, the pronounced decline in these enzyme activities in the late
404 LG stage occurred despite relatively abundant soil nutrients pools, indicating that internal
405 microbial stoichiometric imbalances progressively overrode external substrate availability
406 as the primary constraint on enzyme metabolism. This successional shift was consistent with
407 previous findings in subtropical forest restoration ecosystems (Feng et al., 2019; Zhang et
408 al., 2022, Wan et al., 2025).

409 Notably, BG, NAG, and ACP exhibited divergent sensitivities to substrate supply and
410 microbial stoichiometric status. ACP activity was strongly negatively correlated with
411 MBC:P ratio ($r = –0.822$, $p < 0.01$; Table S3), indicating that microbial P acquisition strategy
412 was directly impacted by intracellular P status. In LG, the significantly elevated MBC:P
413 indicated aggravated microbial P deficiency. Under severe and persistent P limitation, soil
414 microbes tend to shift from extracellular P mining to intracellular P conservation, including
415 reducing ribosomal RNA synthesis and recycling internal nucleic acid P, thereby decreasing
416 synthesis of energy-costly ACP (Sinsabaugh et al., 2009; Manzoni et al., 2012; Schimel &
417 Schaeffer, 2012). By contrast, BG and NAG showed weaker correlations with microbial
418 stoichiometric ratios (MBC:P for BG: $r = –0.584$; MBC:N for NAG: $r = –0.751$; Table S3),
419 implying that microbial C- and N-acquisition strategies depended more on soil substrate
420 availability than internal stoichiometric status (Allison et al., 2011; Sinsabaugh & Follstad
421 Shah, 2012).

422 The opposite successional trends of CBH and BG reflected differentiated response
423 mechanisms for labile versus recalcitrant C-acquiring enzymes (Fig. 2). BG is responsible

for decomposing labile cellobiose and is mainly induced by readily available C substrates, whereas CBH targets crystalline cellulose and lignocellulose and is highly sensitive to litter structure traits (Sinsabaugh et al., 2008). This functional distinction was borne out by our correlation analyses (Fig. 3, Table S3). BG activity was closely associated with concentrations of labile C substrates (DOC), soil nutrients (TP, AP), and MBC, while CBH was positively correlated with LC:N, soil Fe, and silt content, and negatively correlated with MBC. The positive CBH- LC:N correlation reflects that high-C:N, low-N litter contains more recalcitrant lignocellulose, requiring greater cellulolytic investment (Leitner et al., 2012). The positive association between CBH and soil Fe concentration is attributable to the strong sorption and protective effects of Fe oxides on soil organic matter which modulates enzyme stability and substrate accessibility (Hu et al., 2026; Sheng et al., 2023). Furthermore, the negative CBH-MBC correlation confirmed that robust microbial communities with high biomass preferentially utilize labile C substrates rather than investing in recalcitrant cellulose degradation (Milcu et al., 2011; Michel et al., 2023).

The peak BG activity in CA coincided with the highest DOC and microbial biomass (Tables 2, 3), further verifying substrate-induced enzyme synthesis under sufficient labile C supply. The continuous decline in CBH along the restoration gradient was primarily influenced by successional changes in litter quality. Early-stage coniferous plantations produced high C:N litter rich in cellulose, favoring proliferation of cellulose-degrading microbes. In contrast, late-stage evergreen broadleaved forests generated N-enriched litter with lower cellulose proportions, reducing microbial demand for recalcitrant cellulose decomposition (Krishna & Mohan, 2017; Table 1S). Moreover, intensified C-P co-limitation

446 in LG further suppressed CBH synthesis (Fig. 4b, c). Under dual C and P limitation,
447 microbial resources were preferentially allocated to nutrient acquisition, rather than
448 recalcitrant C degradation, ultimately inhibiting CBH activity. Collectively, the divergent
449 dynamics of BG and CBH (Fig. 2) indicate that microbial C limitation was not uniform
450 across soil C pools; labile and recalcitrant C cycling responded differentially to vegetation
451 restoration.

452 NAG and ACP showed consistent variation trends across the restoration
453 chronosequence, both peaking in CA and declining in LG (Fig. 2). NAG activity was
454 positively associated with FRN and NO_3^--N, reflecting that sufficient available N stimulated
455 N-mining enzyme synthesis under non-limiting N conditions (Liu et al., 2022; Wan et al.,
456 2025). Meanwhile, the negative correlation between NAG and Lsc indicated that thick
457 structurally-complex litter layers hindered enzyme diffusion and substrate contact,
458 physically restricting NAG activity (Weintraub et al., 2012). Similarly, ACP was positively
459 associated with MBC and LTN, reflecting that high microbial biomass and N-rich litter
460 exacerbated P demand via classic N-induced P limitation (Gao et al., 2024), while its
461 negative association with MBC:P further indicated the involvement of microbial P
462 stoichiometry.

463 In LG, elevated MBC:P and persistent P limitation (Fig. 3c) was associated with
464 microbes exhibiting an intracellular resource-conservation strategy, reducing ACP synthesis
465 (Sinsabaugh et al., 2009; Manzoni et al., 2012). The coupled negative correlations of NAG
466 with fine root C:N and ACP with MBC:P together with significantly elevated MBC:N and
467 MBC:P in LG (Table 3), clearly indicate a successional transition of microbial metabolic

strategies: from external nutrient mining in early and middle stages to internal resource conservation in late stages (Cui et al., 2022). This metabolic transition is reinforced by soil physical and chemical constraints: thick surface litter layers likely impeded enzyme diffusion (Weintraub et al., 2012), while abundant clay and Fe/Al oxides in acidic subtropical soils adsorb enzymes and substrates, further reducing measurable ACP activity (Hou et al., 2018). Overall, N- and P-acquiring enzymes activities are jointly affected by external nutrient availability and internal stoichiometric balance, with resource conservation progressively overriding external nutrient acquisition as the dominant microbial strategy in late-stage forests (Moorhead et al., 2016).

4.2 Shift in microbial nutrient limitation along the forest restoration chronosequence

Microbial resource constraint is a universal phenomenon in terrestrial ecosystems, shaped by the integrated effects of soil properties, plant functional traits, and environmental conditions (Tian et al., 2020; Cui et al., 2025). Microbial nutrient constraint determines carbon-use efficiency (CUE) and metabolic turnover, fundamentally affecting soil C sequestration and nutrient biogeochemical cycling (Sinsabaugh & Follstad Shah, 2011; Manzoni et al., 2012). Consistent with our second hypothesis, enzymatic vector analyses demonstrated that subtropical forests succession triggered progressive intensification of microbial C-P co-limitation, rather than resource alleviation. From early coniferous plantations to late evergreen broadleaved forests, vector length increased steadily from 0.63 to 0.79, and vector angle peaked at 80.04° in LG, verifying the strongest C-P co-limitation in late-successional forests (Fig. 4b, c). This successional trajectory of aggravated limitation aligns with recent subtropical forest restoration studies, that reported continuous

strengthening of C limitation and persistent P limitation throughout forest recovery (Zhang et al., 2022; Wan et al., 2025).

The ubiquitous P limitation across all restoration stages is inherent to the pedological characteristics of subtropical acidic red soils. All enzymatic stoichiometric data points fell far below the 55° threshold (Fig. 4a), confirming that microbial metabolism was universally P- rather than N-limited. This finding agrees with large-scale investigations showing that over 80% of Chinese forest soils suffer from severe P limitation (Cui et al., 2022). Mechanistically, highly-weathered subtropical red soils contain abundant Fe and Al oxides and hydroxides that strongly sorb P and reduce its bioavailability; coupled with the inherently low P concentration of parent materials and persistent acidity (pH 4.05-4.26, Table 2), P deficiency becomes a persistent edaphic feature (Waring et al., 2014; Hou et al., 2018). Under such chronic P-deficient conditions, soil microbes prioritize P acquisition and thus maintain cellular stoichiometric status, explaining the consistently greater investment in P-acquiring ACP relative to C- and N-acquiring enzymes across all forest stages (Allison et al., 2011; Xiao et al., 2026). Importantly, recent metagenomic studies have confirmed that soil P limitation suppresses microbial C catabolic activity during vegetation restoration, offering a mechanistic bridge that explains how chronic P deficiency exacerbates C limitation in late-successional forests (Wang et al., 2024).

The gradual intensification of microbial C-P co-limitation in late-stage forests was primarily influenced by the trade-off between litter chemical quality and structural recalcitrance. Although litter C:N and C:P decreased gradually along the restoration gradient (Table S1), suggesting enhanced elemental stoichiometry, late-stage broadleaved litter

512 contained more lignin and condensed tannin, leading to increased structural recalcitrance.
513 The complex physical structure of recalcitrant litter sequesters organic C and reduces
514 substrate accessibility to microbes, ultimately exacerbating C limitation, despite favorable
515 elemental ratios (Sinsabaugh & Follstad Shah, 2011; Krishna & Mohan, 2017). Our random
516 forest and PLS-PM results jointly identified litter quality traits (LTN, LC:N) and microbial
517 biomass stoichiometry (MBN:P and MBC:N) as the core factors associated with microbial
518 C and P limitation, respectively (Figs. 5 and 6). The critical role of litter quality in affecting
519 C limitation highlights that plant-derived organic matter inputs, rather than inherent soil
520 nutrient pools, impact microbial C resource-allocation strategies (Zhang et al., 2022; Wang
521 et al., 2024). For P limitation, the strong predictive power of MBC:N and LC:P indicates that
522 microbial P stress was primarily caused by a stoichiometric mismatch between microbial
523 nutrient demand and substrate supply. Late-stage N-rich but P-poor litter inputs elevated
524 microbial N:P demand imbalance, further intensifying P limitation (Gao et al., 2024). This
525 is consistent with recent findings that tree species identity, rather than species richness per
526 se, impact microbial resource limitation in subtropical mixed plantations, with certain
527 broadleaved species like *Schima superba* effectively alleviating P limitation while others
528 like *Elaeocarpus decipiens* exacerbating C demand (Li et al., 2026). Accumulating evidence
529 suggests that microbial biomass C:N:P stoichiometry is a more sensitive and reliable
530 indicator of microbial nutrient limitation and soil C dynamics than soil or enzymatic
531 stoichiometry alone (Luo et al., 2022). A recent meta-analysis further verified that microbial
532 biomass and its stoichiometric imbalance are key modulators of soil enzymatic responses,
533 acting as both sensors and drivers of ecosystem-scale microbial resource limitation (Liu et

al., 2026).

PLS-PM revealed significant functional decoupling among environmental factors affecting microbial limitation patterns. Soil properties exerted the strongest positive effect on C limitation (total effect = 0.91) but the strongest negative effect on P limitation (total effect = −0.87). This contrasting response indicates that improved soil nutrient pools alleviated P stress by increasing P availability, while simultaneously promoting microbial biomass and metabolic activity, which enhanced C demand and thus intensified C limitation (Wan et al., 2025). Litter properties significantly aggravated P limitation and slightly enhanced C limitation, suggesting that N-rich late-stage litter stimulated microbial proliferation and P demand without corresponding P supply, ultimately exacerbating P limitation (Qiu et al., 2023; Wang et al., 2024). In contrast, fine root inputs alleviated P limitation but intensified C limitation, implying that root-derived C substrate adjusted soil substrate stoichiometry and relieved P stress while aggravating C resource constraints (Duan et al., 2024). Microbial biomass and stoichiometric traits significantly promoted C limitation, confirming that microbial stoichiometric imbalance (Table 3) is both a consequence and a driver of progressive C-P co-limitation during forest succession (Qiu et al., 2023).

Spatial stratification of litter inputs and intensified plant-microbe resource competition further exacerbated late-stage microbial co-limitation. Surface-concentrated litterfall led to uneven vertical distribution of organic matter and P inputs, resulting in lower extracellular enzyme activities and more severe P limitation in subsoil layers (Weintraub et al., 2012). Additionally, different microbial functional groups exhibited divergent resource acquisition strategies, altering intra-community competition and metabolic demands (Crowther et al.,

2019). Even with enhanced soil nutrient pools in restored forests, the rapidly-expanding microbial community escalated metabolic demands, creating a supply-demand mismatch that aggravated nutrient limitation (Deng et al., 2019; Ling et al., 2025). The significant positive correlation between vector angle and soil N:P (Table S3) further confirmed N-induced P limitation, where accumulated N inputs in restored forests amplified microbial P limitation (Pang et al., 2025).

Notably, intensified plant-microbe competition represents a critical and often overlooked factor involved in late-stage co-limitation. With development of aboveground canopy and root systems in late-successional forests, plants competed intensely with microbes for limited soil P, further reducing P bioavailability. Under dual C-P stress, microbes adopted an energy-conservation strategy rather than continuously enhancing enzyme synthesis. The decreased ACP activity in P-deficient LG strongly supports this: severe C-P co-limitation suppressed overall microbial metabolic activity and enzyme synthesis, rather than triggering unlimited upregulation (Manzoni et al., 2012; Moorhead et al., 2016).

5 Conclusions

In our study, we systematically examined the successional trajectories and associated mechanisms of soil microbial metabolic limitation across a typical subtropical forest-restoration chronosequence. Enzymatic vector analysis revealed a progressive intensification of microbial C-P co-limitation, with vector length increasing from 0.63 in early PM to 0.79 in late-stage evergreen broadleaved forests, and vector angle peaking at

80.04° in the LG, indicating the most severe co-limitation occurred in the late-stage (Fig. 7). This intensification was affected by multiple interacting factors: increased litter structural recalcitrance that physically sequestered C, stoichiometric mismatches between microbial demand and substrate supply, intensified plant-microbe competition for limited P, and progressive decoupling between soil nutrient pools and microbial metabolic requirements. Litter quality (LTN and LC:N) emerged as the primary predictor of C limitation, while microbial biomass stoichiometry (MBN:P and MBC:N) predominantly affected P limitation. Soil properties exerted contrasting effects, alleviating P stress while intensifying C limitation by promoting microbial proliferation. These findings demonstrate that forest restoration did not consistently enhance microbial resource availability but instead created metabolic bottlenecks in late-stage that may constrain soil organic matter turnover and long-term carbon sequestration. To sustain soil ecological functions and C sink capacity in restored subtropical forests, targeted management strategies, including introducing tree species with labile stoichiometrically-balanced litter and applying moderate P fertilization, are recommended to mitigate C-P co-limitation.

Statements and Declarations

Funding

This work was financially supported by the Research Funding of Guangxi Academy of Sciences (2024YWF2110), the Guangxi Young Talents Development Program (2025QMJH-0601), the National Natural Science Foundation of China (U23A20154), and the 2025 “Light of Bagui” Visiting Scholarship Program (Young Science and Technology Talents

Special Project) of Guangxi Zhuang Autonomous Region.

Acknowledgments

We extend our sincere gratitude to the staff of the Dashanchong Forest Farm, Changsha County, Hunan Province, for their support.

Author contributions

Jinlei Chen: Data curation, formal analysis, investigation, methodology, visualization, writing-original draft; Xi Fang: Conceptualization, funding acquisition, project administration, resources, supervision, writing-review and editing; Zhiwei Cao: Validation, writing-review and editing; Xiaoye Zhu: Investigation, writing - review and editing; Huiying Lin: Writing-review and editing; Hans Lambers: Writing-review and editing; Xiaoguo Zhou: Writing-review and editing; Junmo Xu: Writing - review and editing; Yongjie Huang: Data curation, validation; Dongjing Sun: Writing - review and editing; Yuanguang Wen: Writing - review and editing; Enqing Hou: Conceptualization, supervision, writing-review and editing.

Competing interests

The authors declare that they have no conflict of interest.

References

Allison VJ, Condron LM, Peltzer DA, Richardson SJ, Turner BL (2007) Changes in enzyme activities and soil microbial community composition along carbon and nutrient gradients at the Franz Josef chronosequence, New Zealand. Soil Biol Biochem 39:1770-1781. https://doi.org/10.1016/j.soilbio.2007.02.006

623 Allison SD, Weintraub MN, Gartner TB, Waldrop MP (2011) Evolutionary-economic principles as
624 regulators of soil enzyme production and ecosystem function. In: Shukla G, Varma A (Eds.), Soil
625 Enzymology. Springer, Berlin.
626 Burke DJ, Weintraub MN, Hewins CR, Kalisz S (2011) Relationship between soil enzyme activities,
627 nutrient cycling and soil fungal communities in a northern hardwood forest. Soil Biol Biochem
628 43:795-803. https://doi.org/10.1016/j.soilbio.2010.12.014
629 Chen C, Fang X, Xiang WH, Lei PF, Ouyang S, Kuzyakov Y (2020) Soil plant co stimulation during
630 forest vegetation restoration in a subtropical area of southern China. For Ecosyst 7:404-
631 420. https://doi.org/10.1186/s40663-020-00242-3
632 Chen H, Li DJ, Zhao J, Zhang W, Xiao KC, Wang KL (2018) Nitrogen addition aggravates microbial
633 carbon limitation: evidence from ecoenzymatic stoichiometry. Geoderma 329:61-
634 68. https://doi.org/10.1016/j.geoderma.2018.05.019
635 Crowther TW, van den Hoogen J, Wan J, Mayes MA, Keiser AD, Mo L, Averill C, Maynard DS (2019)
636 The global soil community and its influence on biogeochemistry. Science
637 365:aav0550. https://www.science.org/doi/10.1126/science.aav0550
638 Cui YX, Fang LC, Guo XB, Han F, Ju WL, Ye LP, Wang X, Tan WF, Zhang XC (2019) Natural grassland
639 as the optimal pattern of vegetation restoration in arid and semi-arid regions: evidence from nutrient
640 limitation of soil microbes. Sci Total Environ 648:388-
641 397. https://doi.org/10.1016/j.scitotenv.2018.08.173
642 Cui YX, Moorhead DL, Guo XB, Peng SS, Wang YQ, Zhang XC, Fang LC (2021) Stoichiometric models
643 of microbial metabolic limitation in soil systems. Glob Ecol Biogeogr 30:2297-
644 2311. https://doi.org/10.1111/geb.13378

Cui YX, Bing HJ, Moorhead DL, Delgado-Baquerizo M, Ye LP, Yu JL, Zhang SP, Wang X, Peng SS, Guo X, Zhu B, Chen J, Tan WF, Wang YQ, Zhang XC, Fang LC (2022) Ecoenzymatic stoichiometry reveals widespread soil phosphorus limitation to microbial metabolism across Chinese forests. Commun Earth Environ 3:184. https://doi.org/10.1038/s43247-022-00523-5

Cui YX, Moorhead DL, Peng SS, Sinsabaugh RL, Peñuelas J (2024) Predicting microbial nutrient limitations from a stoichiometry-based threshold framework. Innovation Geoscience 2:100048. https://doi.org/10.59717/j.xinn-geo.2024.100048

Cui YX, Peng SS, Rillig MC, Camenzind T, Delgado-Baquerizo M, Terrer C, Xu XF, Feng MY, Wang MJ, Fang LC, Zhu B, Du EZ, Moorhead DL, Sinsabaugh RL, Peñuelas J, Elser JJ (2025) Global patterns of nutrient limitation in soil microorganisms. Proc Natl Acad Sci USA 122: e2424552122. https://doi.org/10.1073/pnas.2424552122

Deng L, Wang KB., Chen ML, Shangguan ZP, Sweeney S (2013) Soil organic carbon storage capacity positively related to forest succession on the Loess Plateau, China. Catena 110: 1-7. https://doi.org/10.1016/j.catena.2013.06.016

Deng Q, Cheng XL, Hui DF, Zhang Q, Li M, Zhang Q (2019) Soil microbial community and its interaction with soil carbon and nitrogen dynamics following afforestation in central China. Sci Total Environ 651:282-291. https://doi.org/10.1016/j.scitotenv.2015.09.080

Duan CJ, Fang LC, Yang CL, Chen WB, Cui YX, Li SQ (2018) Reveal the response of enzyme activities to heavy metals through in situ zymography. Ecotoxicol Environ Saf 156:106-115. https://doi.org/10.1016/j.ecoenv.2018.03.015

Duan SL, Guo JP, Zhang YX, Liu LB, Wang R, Zheng RR (2024) Rhizosphere effects and microbial N limitations drive the root N limitations in the rhizosphere during secondary succession in a *Pinus*

667 *tabuliformis* forest in North China. Front Plant Sci
668 15:1392934. https://doi.org/10.3389/fpls.2024.1392934
669 Fan YX, Wu F, Yang YJ, Wang YN, Liu T, Yang T, Mao C, Huang WB, Zhou SS (2025) Tree functional
670 identity drives soil enzyme stoichiometric ratios and microbial nutrient limitation responses to
671 artificial forest conversion. Forests 16:1327. https://doi.org/10.3390/f16081327
672 Feng C, Ma YH, Jin X, Wang Z, Ma Y, Fu SL, Chen HY (2019) Soil enzyme activities increase following
673 restoration of degraded subtropical forests. Geoderma 351:180-
674 187. https://doi.org/10.1016/j.geoderma.2019.05.006
675 Gao K, Du H, Zhu ZH, Fang YT, Li DJ (2024) Increasing plant species diversity aggravates microbial
676 phosphorus limitation but alleviates microbial carbon limitation in a subtropical forest. J Plant Ecol
677 17:rtae100. https://doi.org/10.1093/jpe/rtae100
678 German DP, Weintraub MN, Grandy AS, Lauber CL, Rinkes ZL, Allison SD (2011) Optimization of
679 hydrolytic and oxidative enzyme methods for ecosystem studies. Soil Biol Biochem 43: 1387-1397.
680 https://doi.org/10.1016/j.soilbio.2011.03.017
681 Gong JC, Sun FD, Wu JJ, Zhou SJ, Xiu Y, Li LL, Kausar T, Ma ZW, Zhou JQ, Liu L, Cui YX, Sardans J,
682 Peñuelas J, Elrys A, Chen J, Bai YF (2025) Long-term active rather than passive restoration promotes
683 soil organic carbon accumulation by alleviating microbial nitrogen limitation in an extremely
684 degraded alpine grassland. Adv Sci 13:e10549. https://doi.org/10.1002/advs.202510549
685 Hou EQ, Tang SB, Chen CR, Kuang YW, Lu XK, Heenan M, Wen DZ (2018) Solubility of phosphorus
686 in subtropical forest soils as influenced by low-molecular organic acids and key soil properties.
687 Geoderma 313:172-180. https://doi.org/10.1016/j.geoderma.2017.10.039
688 Hu MY, Dai XQ, Kuzyakov Y, Gao DC, Meng SW, Lyu S, Yang Z, Zhang XY, Fu XL, Kou L, Yang FT,

Wen XF, Wang HM (2026) Iron oxides, enzymes, and nutrients control soil organic matter stability in subtropical forest ecosystems. Geoderma 467:117731. https://doi.org/10.1016/j.geoderma.2026.117731.

Hu N, Li H, Tang Z, Li ZF, Li GC, Jiang Y, Hu XM, Lou YL (2016) Community size, activity and C:N stoichiometry of soil microorganisms following reforestation in a karst region. Eur J Soil Biol 73:77-83. https://doi.org/10.1016/j.ejsobi.2016.01.007

Huang WJ, Liu JX, Wang YP, Zhou GY, Han TF, Li Y (2013) Increasing phosphorus limitation along three successional forests in southern China. Plant Soil 364:181-191. https://doi.org/10.1007/s11104-012-1355-8

Ivanov K, Zaprjanova P, Petkova M, Stefanova V, Kmetov V, Georgieva D, Angelova V (2012) Comparison of inductively coupled plasma mass spectrometry and colorimetric determination of total and extractable phosphorus in soils. *Spectrochim Acta Part B* 71–72: 117-122. https://doi.org/10.1016/j.sab.2012.05.008

Joergensen RG, Mueller T (1996) The fumigation extraction method to estimate soil microbial biomass: calibration of the kEN value. Soil Biol Biochem 28:33-37. https://doi.org/10.1016/0038-0717(95)00101-8

Krishna MP, Mohan M (2017) Litter decomposition in forest ecosystems: a review. Energy Ecol Environ 2:236-249. https://doi.org/10.1007/s40974-017-0064-9

Leitner S, Wanek W, Wild B, Haemmerle I, Kohl L, Keiblinger KM, Zechmeister-Boltenstern S, Richter A (2012) Influence of litter chemistry and stoichiometry on glucan depolymerization during decomposition of beech (*Fagus sylvatica* L.) litter. Soil Biol Biochem 50(6):174-187. https://doi.org/10.1016/j.soilbio.2012.03.012

Li Y, Fang X, Xiang WH, Lei PF, Chen L, Ouyang S, Deng XW, Hu YT, Wu HL (2026) Species identity outweighs richness in shaping soil microbial resource limitation in subtropical mixed *Pinus massoniana* broadleaved plantations. Catena 264:109744. https://doi.org/10.1016/j.catena.2025.109744

Ling J, Dungait JAJ, Delgado-Baquerizo M, Cui ZL, Zhou RR, Zhang WS, Gao Q, Chen YX, Yue SC, Kuzyakov Y, Zhang FS, Chen XQ, Tian J (2025) Soil organic carbon thresholds control fertilizer effects on carbon accrual in croplands worldwide. Nat Commun 16:3009. https://doi.org/10.1038/s41467-025-57981-6

Liu C, Xiang WH, Lei PF, Deng XW, Tian DL, Fang X, Peng CH (2014) Standing fine root mass and production in four Chinese subtropical forests along a succession and species diversity gradient. Plant Soil 376:445-459. https://doi.org/10.1007/s11104-013-1998-0

Liu HH, Ren TT, Liao JH, Chen HYH, Zou XM, Ruan HH (2026) Nitrogen deposition alleviates phosphorus-induced imbalances in soil enzyme stoichiometry. Commun Earth Environ 7:88. https://doi.org/10.1038/s43247-025-03115-1

Liu M, Gan B, Li Q, Xiao W, Song X (2022) Effects of nitrogen and phosphorus addition on soil extracellular enzyme activity and stoichiometry in Chinese fir (*Cunninghamia lanceolata*) forests. Front Plant Sci 13:862184. https://doi.org/10.3389/fpls.2022.834184

Lozano YM, Hortal S, Armas C, Pugnaire FI (2014) Interactions among soil, plants, and microorganisms drive secondary succession in a dry environment. Soil Biol Biochem 78:298-306. https://doi.org/10.1016/j.soilbio.2014.08.007

Luo HQ, Yu JL, Li RX, Gu JD, Luo L, Zhang YY, He Y, Xiao YL, Deng SH, Zhang YZ, Zhang SR, Wang LL, He JS, Deng OP, Lan T (2022) Microbial biomass C:N:P as a better indicator than soil and

733 ecoenzymatic C:N:P for microbial nutrient limitation and C dynamics in Zoige Plateau peatland soils.
734 Appl Soil Ecol 175:104348. https://doi.org/10.1016/j.ibiod.2022.105492
735 Manzoni S, Taylor P, Richter A, Porporato A, Ågren GI (2012) Environmental and stoichiometric controls
736 on microbial carbon use efficiency in soils. New Phytol 196:79-91. https://doi.org/10.1111/j.1469-
737 8137.2012.04225.x
738 Michel J, Hartley IP, Buckeridge KM, Van Meegen C, Broyd RC, Reinelt L, Ccahuana Quispe AJ,
739 Whitaker J (2023) Preferential substrate use decreases priming effects in contrasting treeline soils.
740 Biogeochemistry 162:141-161. https://doi.org/10.1007/s10533-022-00996-8
741 Milcu A, Heim A, Ellis RJ, Scheu S, Manning P (2011) Identification of general patterns of nutrient and
742 labile carbon control on soil carbon dynamics across a successional gradient. Ecosystems 14:710-
743 719. https://doi.org/10.1007/s10021-011-9440-z
744 Moorhead DL, Sinsabaugh RL, Hill BH, Weintraub MN (2016) Vector analysis of ecoenzyme activities
745 reveal constraints on coupled C, N and P dynamics. Soil Biol Biochem 93:1-
746 7. https://doi.org/10.1016/j.soilbio.2015.10.019
747 Mori T (2020) Does ecoenzymatic stoichiometry really determine microbial nutrient limitations? Soil
748 Biol Biochem 146:107816. https://doi.org/10.1016/j.soilbio.2020.107816
749 Mori T (2024) Is enzymatic stoichiometry a reliable indicator of microbial limitations in carbon, nitrogen,
750 or phosphorus? Sci Total Environ 955:176928. https://doi.org/10.1016/j.scitotenv.2024.176928
751 Pang CL, Zhang ZH, Zhu XM, Wei WT, Mustafa A, Chen WB, Mao QG, Mo JM, Li S, Lu XK (2025)
752 Divergent microbial metabolic limitations across soil depths after two decades of high nitrogen
753 inputs in a primary tropical forest. Glob Change Biol 31:e70440. https://doi.org/10.1111/gcb.70440
754 Qiu LJ, Li YJ, Zhong Q, Ma W, Kuang YX, Zhou SX, Chen G, Xie JL, Hu YQ, Tu LH (2023) Adaptation

mechanisms of the soil microbial community under stoichiometric imbalances and nutrient-limiting conditions in a subtropical nitrogen-saturated forest. Plant Soil 489:239-258. https://doi.org/10.1007/s11104-023-06014-6

Raiesi F (2012) Soil properties and C dynamics in abandoned and cultivated farmlands in a semi arid ecosystem. Plant Soil 351:161-175. https://doi.org/10.1007/s11104-011-0941-5

Saiya-Cork KR, Sinsabaugh RL, Zak DR (2002) The effects of long term nitrogen deposition on extracellular enzyme activity in an Acer saccharum forest soil. Soil Biol Biochem 34:1309-1315. https://doi.org/10.1016/S0038-0717(02)00074-3

Schimel JP, Schaeffer SM (2012) Microbial control over carbon cycling in soil. Front Microbiol 3:348. https://doi.org/10.3389/fmicb.2012.00348

Sinsabaugh RL, Follstad Shah JJ (2012) Ecoenzymatic stoichiometry and ecological theory. Annu Rev Ecol Evol Syst 43:313-343. https://doi.org/10.1146/annurev-ecolsys-071112-124414

Sinsabaugh RL, Lauber CL, Weintraub MN, Ahmed B, Allison SD, Crenshaw C, Contosta AR, Cusack D, Frey S, Gallo ME, Gartner TB, Hobbie SE, Holland K, Keeler BL, Powers JS, Stursova M, Takacs-Vesbach C, Waldrop MP, Wallenstein MD, Zak DR, Zeglin LH (2008) Stoichiometry of soil enzyme activity at global scale. Ecol Lett 11:1252-1264. https://doi.org/10.1111/j.1461-0248.2008.01245.x

Sinsabaugh RL, Hill BH, Follstad Shah JJ (2009) Ecoenzymatic stoichiometry of microbial organic nutrient acquisition in soil and sediment. Nature 462:795-798. https://doi.org/10.1038/nature08632

Sinsabaugh RL, Follstad Shah JJ (2011) Ecoenzymatic stoichiometry of recalcitrant organic matter decomposition: the growth rate hypothesis in reverse. Biogeochemistry 102:31-43. https://doi.org/10.1007/s10533-010-9482-x

Sheng YZ, Hu JL, Kukkadapu R, Guo DY, Zeng Q, Dong HL (2023) Inhibition of extracellular enzyme activity by reactive oxygen species upon oxygenation of reduced iron-bearing minerals. Environ Sci Technol 57:3204-3214. https://doi.org/10.1021/acs.est.2c09634.

Sterner RW, Elser JJ (2002) Ecological stoichiometry: the biology of elements from molecules to the biosphere. Princeton University Press.

Tian P, Razavi BS, Zhang XC, Wang QK, Blagodatskaya E (2020) Microbial growth and enzyme kinetics in rhizosphere hotspots are modulated by soil organics and nutrient availability. Soil Biol Biochem 141:107662. https://doi.org/10.1016/j.soilbio.2019.107662

Traoré OYA, Kiba DI, Arnold MC, Fliessbach A, Oberholzer HR, Nacro HB, Lompo F, Oberson A, Frossard E, Bünemann EK (2016) Fertilization practices alter microbial nutrient limitations after alleviation of carbon limitation in a Ferric Acrisol. Biol Fertil Soils 52:177-189. https://doi.org/10.1007/s00374-015-1061-9

Turner BL, Lambers H, Wen Z, Auer Y-M, Kandeler E (2024) Microbial nutrient limitation along a 2-million-year dune chronosequence. Soil Biol Biochem 192:109385. https://doi.org/10.1016/j.soilbio.2024.109385

Wan J, Zhang R, Jiang W, Chen YF, Yang J, Hu BA, Ouyang S (2025) Eco enzymatic stoichiometry unveils resource limitations in soil microorganisms during subtropical vegetation restoration. J Appl Ecol 62:2569-2581. https://doi.org/10.1111/1365-2664.70145

Wang HC, Wang H, Crowther TW, Kazuo I, Reich PB, Ryunosuke T, Shi WY (2024) Metagenomic insights into inhibition of soil microbial carbon metabolism by phosphorus limitation during vegetation succession. ISME Commun 4:ycae128. https://doi.org/10.1093/ismeco/ycae128

Wang WY, Ding SJ, Guo TF, Xu XP, He P, Huang SM (2026) Organic amendment strategies differentially

regulate microbial carbon use efficiency: A long term field study integrating microorganism and enzymatic stoichiometry. Agric Ecosyst Environ 397:110051. https://doi.org/10.1016/j.agee.2025.110051

Waring BG, Weintraub SR, Sinsabaugh RL (2014) Ecoenzymatic stoichiometry of microbial nutrient acquisition in tropical soils. Biogeochemistry 117:101-113. https://doi.org/10.1007/s10533-013-9849-x

Weintraub SR, Wieder WR, Cleveland CC, Townsend AR (2012) Organic matter inputs shift soil enzyme activity and allocation patterns in a wet tropical forest. Biogeochemistry 114:313-326. https://doi.org/10.1007/s10533-012-9812-2

Wu J, He ZL, Wei WX, O'Donnell AG, Syers JK (2000) Quantifying microbial biomass phosphorus in acid soils. *Biol Fertil Soils* 32: 500–507. https://doi.org/10.1007/s0037 40000284.

Xiao L, Liu GB, Li P, Li Q, Xue S (2020) Ecoenzymatic stoichiometry and microbial nutrient limitation during secondary succession of natural grassland on the Loess Plateau, China. Soil Tillage Res 200:104605. https://doi.org/10.1016/j.still.2020.104605

Xiao KC, Duan PP, Li DJ (2026) Lithological controls on soil microbial resource limitation in subtropical forests of southwest China. Catena 272:110317. https://doi.org/10.1016/j.catena.2026.110317

Yang YJ, Xia W, Fan YX, Chong YJ, Xiong JT, Yu WJ (2024) Restoring subtropical forests: alleviating P limitation and introducing C limitation using evergreen broad leaved tree species. Forests 15:568. https://doi.org/10.3390/f15030568

Zhang S, Wang YP, Fang X, Chen JL, Cao NN, Xu PP, Yu MX, Xiong X, Tan XP, Deng Q, Yan JH (2022) Plant above ground biomass and litter quality drive soil microbial metabolic limitations during vegetation restoration of subtropical forests. Soil Ecol Lett

5:220154. https://doi.org/10.1007/s42832-022-0154-2

Zhao ZW, Wu Y, Chen WJ, Sun W, Wang ZH, Liu GB, Xue S (2023) Soil enzyme kinetics and thermodynamics in response to long-term vegetation succession. Sci Total Environ 882:163542. https://doi.org/10.1016/j.scitotenv.2023.163542

Figure 1. Location and plot distribution of the study area. PM, *Pinus massoniana* plantation; PL, *Pinus massoniana-Lithocarpus glaber* mixed broadleaved-conifer forest; CA, *Choerospondias axillaris* deciduous broadleaved forest; LG, *Lithocarpus glaber* evergreen broad-leaved forest.

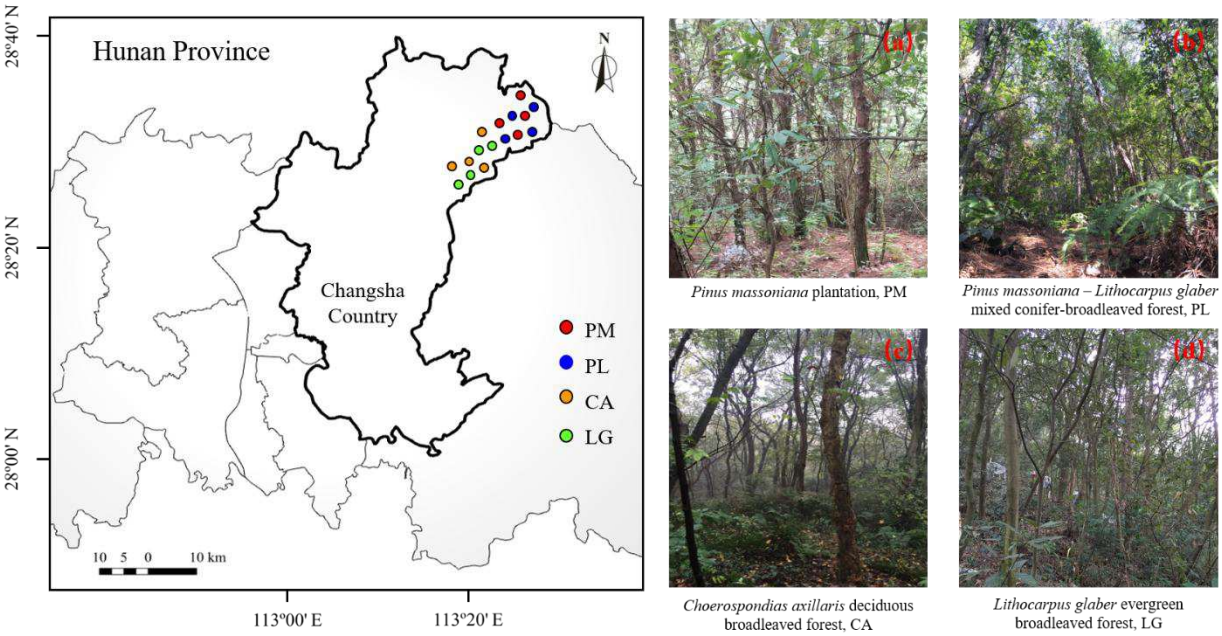


Figure 2. Changes in soil extracellular enzyme activities at different vegetation restoration stages. PM, *Pinus massoniana* plantation; PL, *Pinus massoniana-Lithocarpus glaber* mixed broadleaved-conifer forest; CA, *Choerospondias axillaris* deciduous broadleaved forest; LG, *Lithocarpus glaber* evergreen broad-leaved forest. BG, β-D-glucosidase; CBH, cellobiohydrolase; NAG, β-N-acetylglucosaminidase; ACP, acid phosphatase. Different lowercase letters in the same column indicate significant differences ($p < 0.05$) among the stages based on one-way ANOVA followed by LSD test (n = 4).

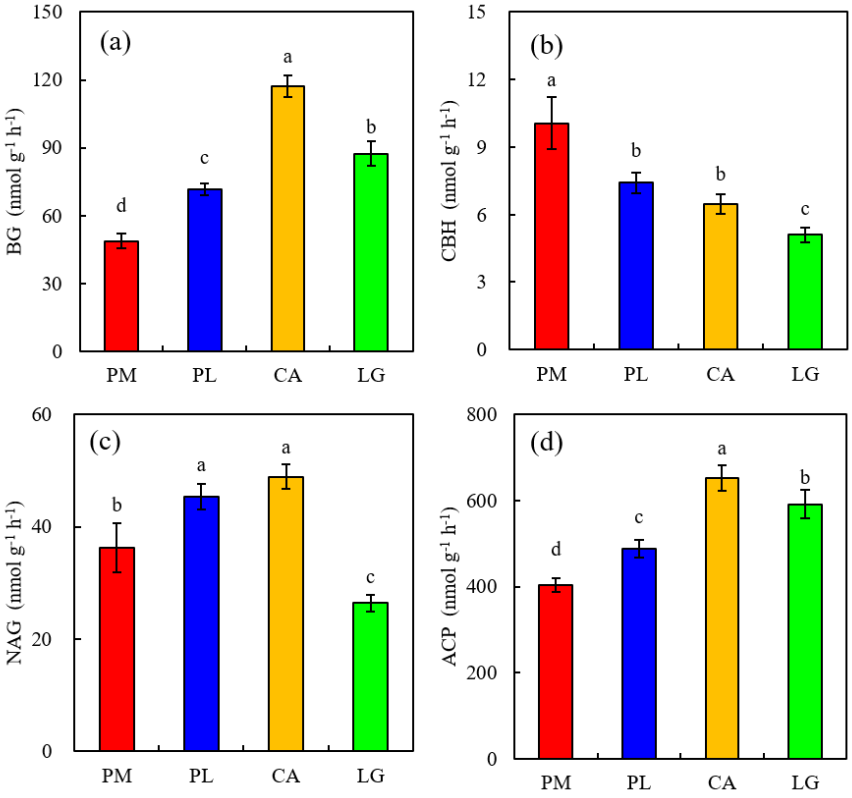
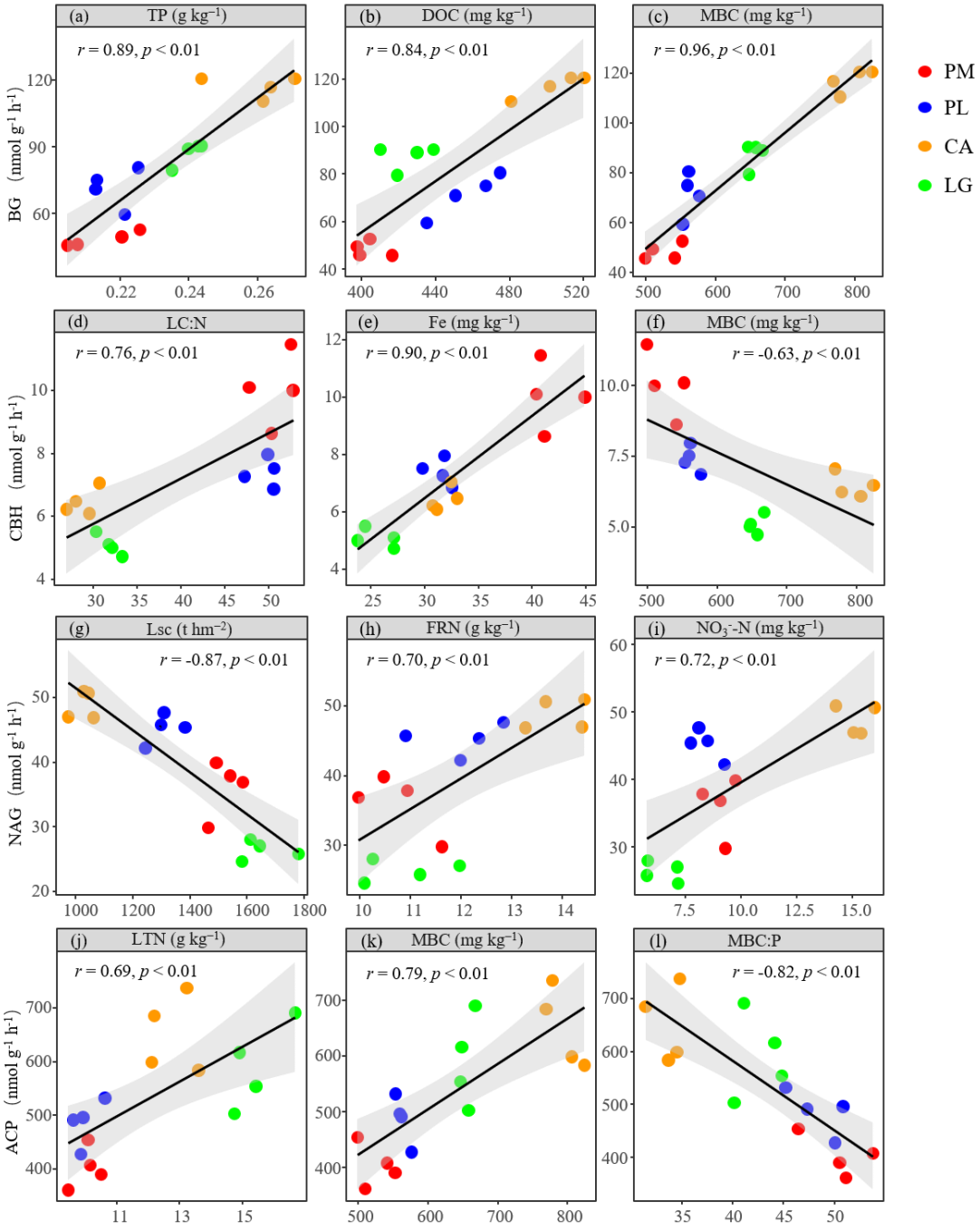


Figure 3. Linear correlation between soil enzyme activities and environmental factors. Panels a, b and c show the correlations between BG and key driving factors (TP, DOC, and MBC); panels d, e and f present the correlations between CBH and key driving factors (LC:N, Fe, and MBC); panels g, h and i illustrate the correlations between NAG and key driving factors (Lsc, FRN, and NO_3^--N); and panels j, k and l display the correlations between ACP and key driving factors (LTN, MBC, and MBC:P). BG, β-D-glucosidase; CBH, cellobiohydrolase; NAG, β-N-acetylglucosaminidase; ACP, acid phosphatase. Lsc, litter layer standing crop; LTN, litter total nitrogen; LC:N, litter organic carbon - total nitrogen ratio; FRN, fine root nitrogen; TP, total phosphorus; DOC, dissolved organic carbon; NO_3^--N, nitrate nitrogen; Fe, total ferruml; MBC, microbial biomass carbon; MBC:P, microbial biomass carbon - phosphorus ratio. The *r* values represent Pearson



correlation coefficients, and *p* values indicate statistical significance.

Figure 4. Extracellular enzyme stoichiometry of the relative proportions of carbon (C) to nitrogen (N) acquisition versus C to phosphorus (P) acquisition (a), the variation of vector length and angle (b and c), and their correlations (d). $TER_{C:N}$ (e) and $TER_{C:P}$ (f) in different vegetation restoration stages. PM, *Pinus massoniana* plantation; PL, *Pinus massoniana-Lithocarpus glaber* mixed broadleaved-conifer forest; CA, *Choerospondias axillaris* deciduous broadleaved forest; LG, *Lithocarpus glaber* evergreen broad-leaved forest. BG, β-D-glucosidase; CBH, cellobiohydrolase; NAG, β-N-acetylglucosaminidase; ACP, acid phosphatase; $TER_{C:N}$, the threshold elemental ratios for C:N; $TER_{C:P}$, the threshold elemental ratios for C:P. Different lowercase letters in the same column indicate significant differences ($p < 0.05$) amongst the stages based on one-way ANOVA followed by LSD test (n = 4).

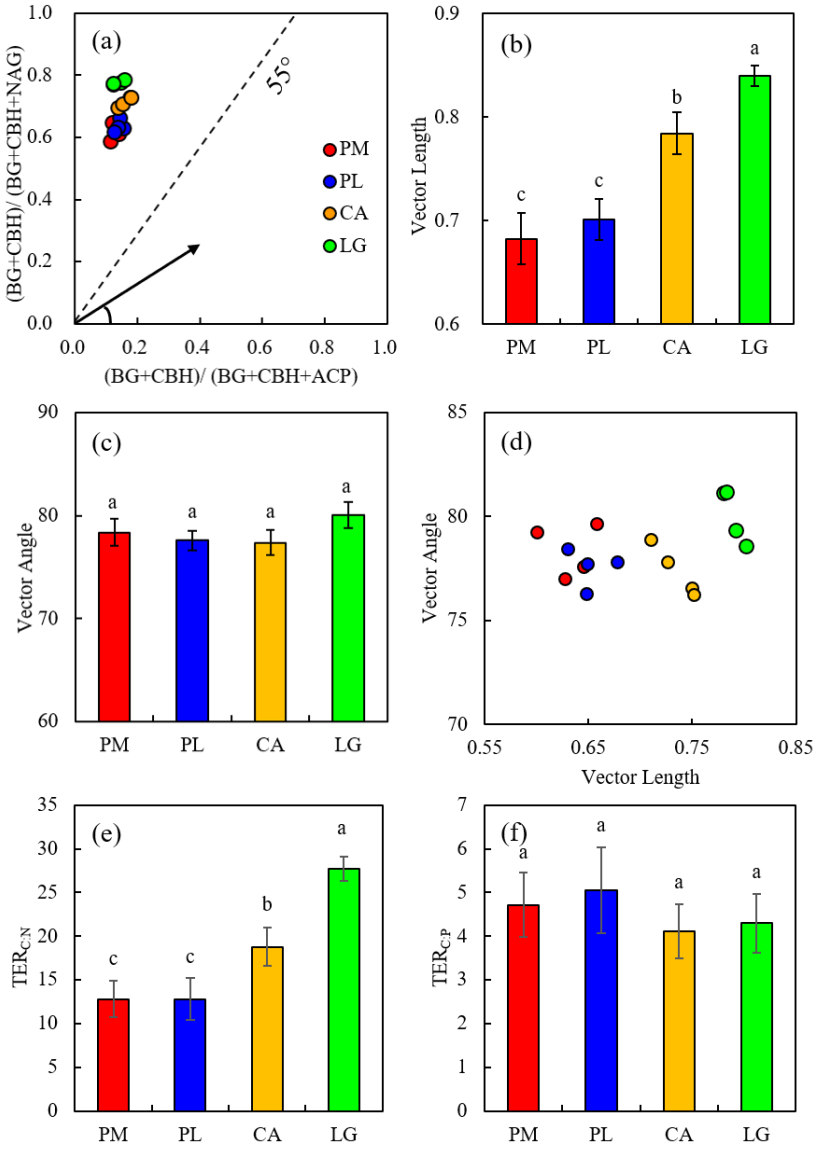


Figure 5. Random forest analysis indicating the relative importance of environmental factors to carbon (C) limitation and phosphorus (P) limitation. H, Shannon-Wiener index; Lsc, litter layer standing crop; LOC, litter organic carbon; LTN, litter total nitrogen; LTP, litter total phosphorus; LC:N, litter organic carbon - total nitrogen ratio; LC:P, litter organic carbon - total phosphorus ratio; LN:P, litter total nitrogen - total phosphorus ratio; FRB, fine root biomass; FROC, fine root organic carbon; FRN, fine root nitrogen; FRP, fine root phosphorus; FC:N, fine root organic carbon - total nitrogen ratio; FC:P, fine root organic carbon - total phosphorus ratio; FN:P, fine root total nitrogen - total phosphorus ratio; MC, Moisture content; BD, bulk density; Sand, >0.02mm sand percentage; Silt, 0.002-0.02mm silt percentage; Clay, <0.002mm clay percentage; pH, soil pH value; SOC, soil organic carbon; TN, total nitrogen; TP, total phosphorus; C:N, soil organic carbon - total nitrogen ratio; C:P, soil organic carbon - total phosphorus ratio; N:P, soil total nitrogen - total phosphorus ratio; DOC, dissolved organic carbon; NH_4^+-N, ammonium nitrogen; NO_3^--N, nitrate nitrogen; AP, available phosphorus; Fe, total ferruml; Al, total aluminum; MBC, microbial biomass carbon; MBN, microbial biomass nitrogen; MBP, microbial biomass P; MBC:N, microbial biomass C - nitrogen ratio; MBC:P, microbial biomass C - P ratio; MBN:P, microbial biomass nitrogen - P ratio.

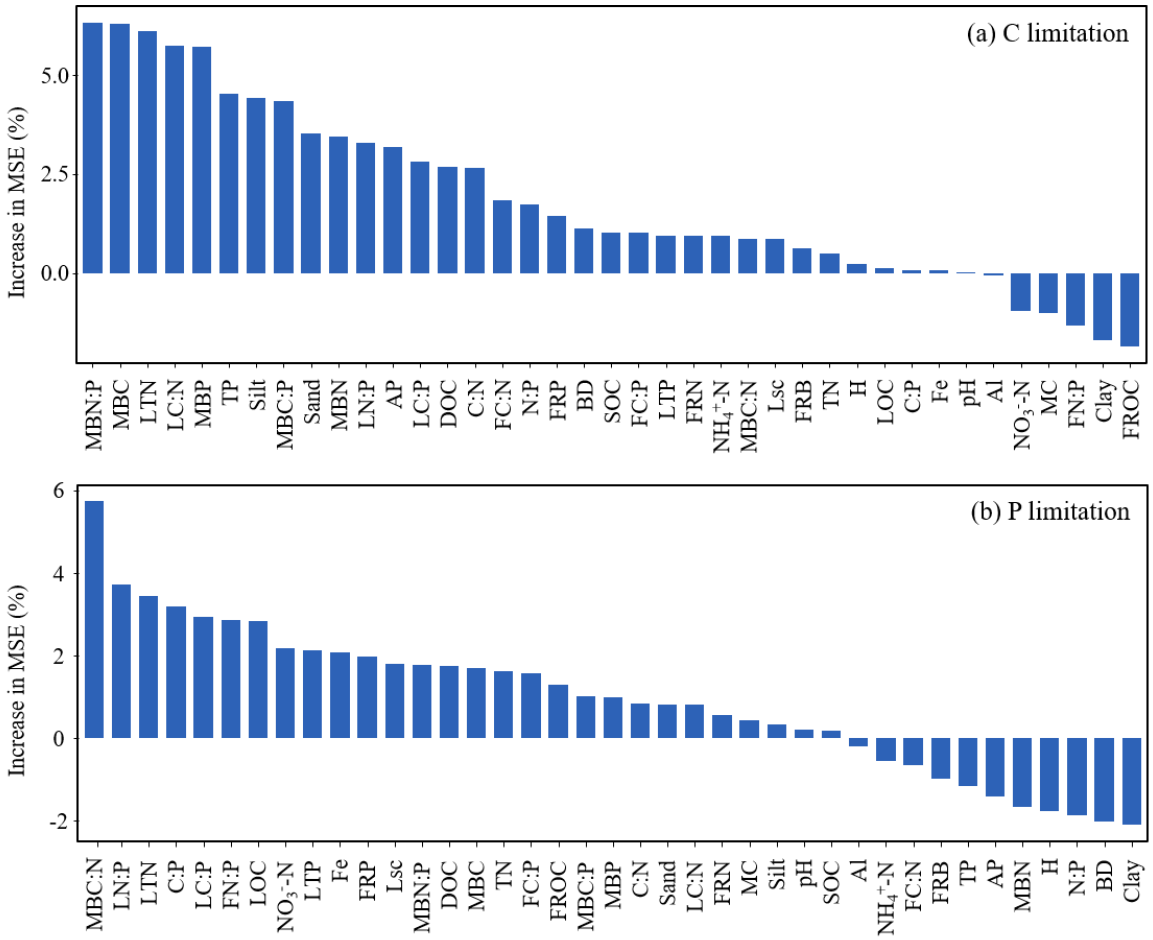


Figure 6. Partial least squares path modeling (PLS-PM) analysis of direct and indirect effects of litter, fine root, soil and microbial properties on carbon (C) limitation (a) and phosphorus (P) limitation (c), with decomposition of total effects for C limitation (b) and P limitation (d). Red and blue arrows represent positive and negative effects, respectively. Solid and dashed lines indicate significant and non-significant pathways, respectively, with numbers along the arrows indicating standardized path coefficients. R^2 denotes the proportion of variance in the dependent variables explained by the model. Significance level: $*p < 0.05$; $**p < 0.01$. LTP, litter total phosphorus; LN:P, litter total nitrogen - total phosphorus ratio; FROC, fine root organic carbon; FRN, fine root nitrogen; FN:P, fine root total nitrogen - total phosphorus ratio; MC, Moisture content; Silt, 0.002-0.02mm silt percentage; pH, soil pH value; C:N, soil organic carbon - total nitrogen ratio; C:P, soil organic carbon - total phosphorus ratio; DOC, dissolved organic carbon; NH_4^+-N, ammonium nitrogen; AP, available phosphorus; MBC:N, microbial biomass C - nitrogen ratio.

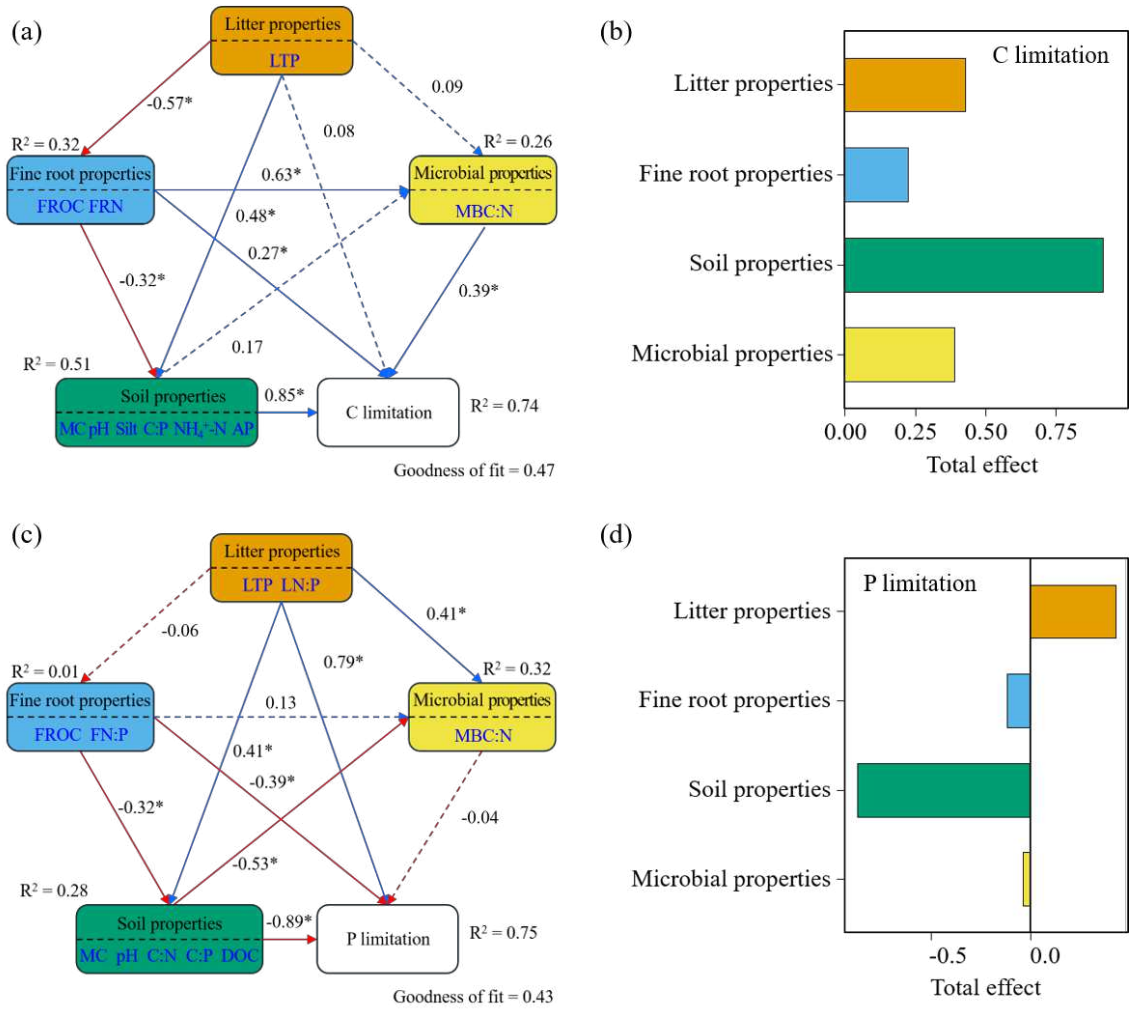
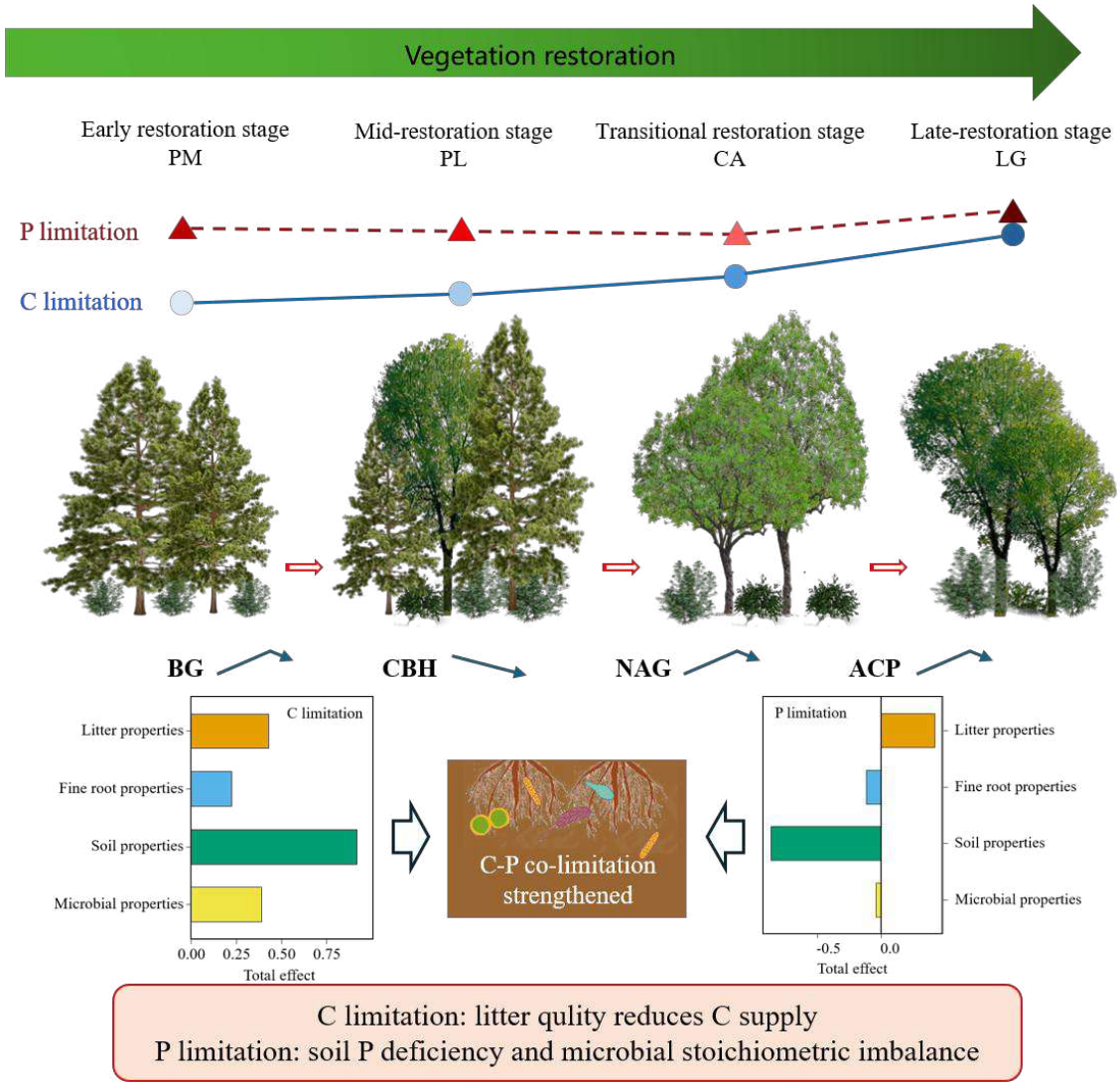


Figure 7. Conceptual diagram of eco-enzymatic stoichiometry revealing microbial resource limitation during vegetation restoration. PM, *Pinus massoniana* plantation; PL, *Pinus massoniana-Lithocarpus glaber* mixed broadleaved-conifer forest; CA, *Choerospondias axillaris* deciduous broadleaved forest; LG, *Lithocarpus glaber* evergreen broad-leaved forest. C limitation, carbon limitation; P limitation, phosphorus limitation. BG, β-D-glucosidase; CBH, cellobiohydrolase; NAG, β-N-acetylglucosaminidase; ACP, acid phosphatase.



899 **Table 1 Stand characteristics of vegetation restoration stages**

Vegetation restoration stage	Forest age (year)	Dominant species	Woody plant density (individuals ha^{-1})	Elevation (m)	Slope aspect	Slope
Pinus massoniana plantation (early restoration stage, PM)	30-35	*Pinus massoniana* *Lithocarpus glaber* *Loropetalum chinense* *Choerospondias axillaris* Others (18 species)	2727	70–125	East	25–30°
Pinus massoniana and *Lithocarpus glaber* mixed coniferous- broadleaved forest (mid-restoration stage, PL)	45-50	*Pinus massoniana* *Lithocarpus glaber* *Cinnamomum camphora* *Choerospondias axillaris* Others (23 species)	2361	75–110	Southeast	18–20°
Choerospondias axillaris deciduous broadleaved forest (transitional stage, CA)	60-70	*Choerospondias axillaris* *Quercus fabri* *Sapindus mukorossi* *Loropetalum chinense* Others (20 species)	1085	52–153	East	25–30°
Lithocarpus glaber evergreen broadleaved forest (late-restoration stage, LG)	80-90	*Lithocarpus glaber* *Pinus massoniana* *Choerospondias axillaris* *Cleyera japonica* Others (28 species)	2116	50–105	Southeast	20–25°

900 Note: Data are based on woody plants with a diameter at breast height of ≥ 4 cm.
901
902

Table 2 Soil physical and chemical properties during vegetation restoration

Soil properties	PM	PL	CA	LG
BD (g cm^{-3})	1.2 ± 0.1 a	1.2 ± 0.1 a	1.1 ± 0.1 b	1.2 ± 0.1 ab
Clay (%)	21.1 ± 3.2 c	28.0 ± 2.0 b	29.1 ± 3.9 b	33.8 ± 1.8 a
Silt (%)	68.1 ± 1.8 a	62.7 ± 1.2 b	61.7 ± 3.1 b	57.7 ± 1.8 c
Sand (%)	10.8 ± 1.6 a	9.3 ± 0.9 ab	9.3 ± 0.9 ab	8.4 ± 0.1 b
pH	4.1 ± 0.1 c	4.0 ± 0.1 c	4.3 ± 0.1 a	4.2 ± 0.1 b
SOC (g kg^{-1})	18.0 ± 1.5 b	17.6 ± 0.5 b	26.6 ± 3.8 a	18.5 ± 1.4 b
TN (g kg^{-1})	1.6 ± 0.1 a	1.2 ± 0.1 b	1.7 ± 0.1 a	1.3 ± 0.2 b
TP (g kg^{-1})	0.21 ± 0.02 c	0.22 ± 0.02 c	0.26 ± 0.02 a	0.24 ± 0.01 b
C:N	11.0 ± 0.9 b	14.3 ± 1.0 a	15.6 ± 1.9 a	14.1 ± 0.3 a
C:P	84.2 ± 10.2 b	80.7 ± 3.0 b	102.2 ± 11.9 a	77.0 ± 5.8 b
N:P	7.6 ± 0.5 a	5.7 ± 0.4 c	6.6 ± 0.3 b	5.4 ± 0.3 c
DOC (mg kg^{-1})	404.3 ± 39.4 c	456.9 ± 17.6 b	503.8 ± 29.0 a	424.5 ± 12.5 bc
NH_4^+-N (mg kg^{-1})	20.1 ± 2.5 a	19.8 ± 2.7 a	19.4 ± 1.4 a	16.8 ± 3.2 a
NO_3^--N (mg kg^{-1})	9.1 ± 1.5 b	8.4 ± 1.2 b	15.2 ± 0.7 a	6. 5 ± 0.8 c
AP (mg kg^{-1})	1.7 ± 0.1 c	2.1 ± 0.02 b	2.3 ± 0.1 a	2.2 ± 0.1 a

Note: Values are means ± standard deviation (n = 4). BD, soil bulk density; Clay, <0.002 mm clay percentage; Silt, 0.002-0.02 mm silt percentage; Sand, >0.02 mm sand percentage; SOC, soil organic carbon; TN, total nitrogen; TP, total phosphorus; C:N, soil organic carbon - total nitrogen ratio; C:P, soil organic carbon - total phosphorus ratio; N:P, soil total nitrogen - total phosphorus ratio; DOC, dissolved organic carbon; NH_4^+-N, ammonium nitrogen; NO_3^--N, nitrate nitrogen; AP, available phosphorus. PM, *Pinus massoniana* plantation; PL, *Pinus massoniana-Lithocarpus glaber* mixed broadleaved-conifer forest; CA, *Choerospondias axillaris* deciduous broadleaved forest; LG, *Lithocarpus glaber* evergreen broad-leaved forest. Different lowercase letters in the same column indicate significant differences (p < 0.05) amongst the stages based on one-way ANOVA followed by LSD test.

915 **Table 3 The average concentrations and ratios of soil microbial biomass across vegetation**
916 **restoration stages**

Microbial properties	PM	PL	CA	LG
MBC (mg kg^{-1})	525.1 ± 25.4 c	562.2 ± 9.9 c	794.3 ± 25.4 a	654.6 ± 9.7 b
MBN (mg kg^{-1})	59.7 ± 2.4 c	68.5 ± 2.9 b	95.1 ± 1.8 a	73.2 ± 2.6 b
MBP (mg kg^{-1})	10.4 ± 0.5 c	11.7 ± 0.5 c	23.7 ± 1.0 a	15.4 ± 1.0 b
MBC:N	8.8 ± 0.5 a	8.2 ± 0.4 b	8.4 ± 0.3 b	9.0± 0.4 a
MBC:P	50.5 ± 3.0 a	48.3 ± 2.6 a	33.6 ± 1.5 c	42.5 ± 2.3 b
MBN:P	5.7 ± 0.1 a	5.9 ± 0.2 a	4.0 ± 0.2 c	4.8 ± 0.3 b

917 Note: Values are means ± standard deviation (n = 4). MBC: soil microbial biomass carbon; MBN: soil
918 microbial biomass nitrogen; MBP: soil microbial biomass phosphorus; MBC:N, microbial biomass carbon
919 - nitrogen ratio; MBC:P, microbial biomass carbon - phosphorus ratio; MBN:P, microbial biomass nitrogen -
920 phosphorus ratio. PM, *Pinus massoniana* plantation; PL, *Pinus massoniana-Lithocarpus glaber* mixed
921 broadleaved-conifer forest; CA, *Choerospondias axillaris* deciduous broadleaved forest; LG, *Lithocarpus*
922 *glaber* evergreen broad-leaved forest. Different lowercase letters in the same column indicate significant
923 differences ($p < 0.05$) amongst the stages based on one-way ANOVA followed by LSD test.
924
925

Supplementary tables and figures

Table S1 The standing crop, carbon, nitrogen, phosphorus concentrations and stoichiometric ratios of litter fall layers in different vegetation restoration stages

Litter properties	PM	PL	CA	LG
Lsc (t ha^{-1})	15.2 ± 3.4 ab	13.1 ± 2.6 c	10.3 ± 1.0 c	16.5 ± 0.9 a
LOC (g kg^{-1})	509.1 ± 29.5 a	494.4 ± 38.1 a	366.8 ± 10.2 b	491.3 ± 13.8 a
LTN (g kg^{-1})	10.0 ± 1.2 c	10.0 ± 0.4 c	12.8 ± 1.9 b	15.4 ± 0.9 a
LTP (g kg^{-1})	0.3 ± 0.03 b	0.3 ± 0.03 b	0.4 ± 0.04 a	0.3 ± 0.02 b
LC:N	51.1 ± 1.4 a	49.5 ± 3.3 a	29.1 ± 3.8 b	31.9 ± 1.2 b
LC:P	1726.8 ± 20.2 a	1768.6 ± 17.2 a	1067.3 ± 37.4 b	1597.8 ± 61.4 a
LN:P	35.4 ± 1.3 b	35.7 ± 2.4 b	36.9 ± 2.4 b	50.2 ± 1.7 a

Note: Values are means ± standard deviation (n = 4). Lsc, litter layer standing crop; LOC, litter organic carbon; LTN, litter total nitrogen; LTP, litter total phosphorus; LC:N, litter organic carbon - total nitrogen ratio; LC:P, litter organic carbon - total phosphorus ratio; LN:P, litter total nitrogen - total phosphorus ratio. PM, *Pinus massoniana* plantation; PL, *Pinus massoniana-Lithocarpus glaber* mixed broadleaved-conifer forest; CA, *Choerospondias axillaris* deciduous broadleaved forest; LG, *Lithocarpus glaber* evergreen broad-leaved forest. Different lowercase letters indicate significant differences among different vegetation restoration stages ($p < 0.05$).

Table S2 Biomass, carbon, nitrogen, phosphorus concentrations and stoichiometric ratios of fine root in different vegetation restoration stages

Fine root properties	PM	PL	CA	LG
FRB (t ha^{-1})	2.5 ± 0.1 b	2.7 ± 0.2 b	2.6 ± 0.2 b	2.8 ± 0.3 a
FROC (g kg^{-1})	447.5 ± 26.8 a	451.7 ± 17.5 a	429.5 ± 28.7 b	456.3 ± 11.3 a
FRN (g kg^{-1})	10.7 ± 1.3 b	12.0 ± 1.4 ab	13.9 ± 1.2 a	10.9 ± 0.9 b
FRP (g kg^{-1})	0.2 ± 0.02 b	0.2 ± 0.01 b	0.3 ± 0.01 a	0.2 ± 0.01 b
FC:N	41.8 ± 3.0 a	37.8 ± 3.8 a	30.9 ± 3.1 b	42.2 ± 3.3 a
FC:P	2400.2 ± 102.8 b	2427.7 ± 108.9 b	1735.2 ± 99.9 c	2699.5 ± 280.4 a
FN:P	57.5 ± 2.1 ab	64..7 ± 6.5 a	56.3 ± 2.3 b	64.3 ± 8.0 a

Note: Values are means ± standard deviation (n = 4). FRB, fine root biomass; FROC, fine root organic carbon; FRN, fine root nitrogen; FRP, fine root phosphorus; FC:N, fine root organic carbon - total nitrogen ratio; FC:P, fine root organic carbon - total phosphorus ratio; FN:P, fine root total nitrogen - total phosphorus ratio. PM, *Pinus massoniana* plantation; PL, *Pinus massoniana-Lithocarpus glaber* mixed broadleaved-conifer forest; CA, *Choerospondias axillaris* deciduous broadleaved forest; LG, *Lithocarpus glaber* evergreen broad-leaved forest. Different lowercase letters indicate significant differences among different vegetation restoration stages ($p < 0.05$).

Table S3. Pearson correlations between enzyme activities, ecological stoichiometric characteristics, microbial nutrient limitations, and environmental factors during vegetation restoration

Environmental factors	BG	CBH	NAG	ACP	EC:N	EC:P	EN:P	Vector Length	Vector Angle	$TER_{C:N}$	$TER_{C:P}$
H	0.174	0.341	0.421	0.208	-0.292	0.023	0.197	-0.196	-0.161	-0.294	-0.359
Lsc	-0.585*	0.042	-0.870**	-0.427	0.268	-0.432	-0.337	0.104	0.526*	0.335	0.159
LOC	-0.857**	0.352	-0.580*	-0.658**	-0.214	-0.601*	0.070	-0.358	0.354	-0.149	0.281
LTN	0.552*	-0.778**	-0.497	0.685**	0.925**	0.080	-0.909**	0.916**	0.539*	0.908**	-0.444
LTP	0.658**	-0.333	0.248	0.680**	0.321	0.225	-0.358	0.427	0.054	0.265	-0.586*
LC:N	-0.864**	0.764**	0.055	-0.852**	-0.795**	-0.381	0.708**	-0.868**	-0.204	-0.747**	0.485
LC:P	-0.834**	0.393	-0.437	-0.744**	-0.313	-0.444	0.257	-0.448	0.144	-0.246	0.490
LN:P	0.275	-0.720**	-0.717**	0.411	0.897**	-0.027	-0.857**	0.829**	0.592*	0.910**	-0.191
FRB	0.240	-0.736**	-0.401	0.295	0.620*	0.036	-0.556*	0.596*	0.318	0.630**	-0.115
FROC	-0.316	-0.073	-0.414	-0.498*	0.112	0.078	0.060	0.055	-0.128	0.162	0.403
FRN	0.699**	-0.280	0.700**	0.520*	-0.008	0.486	0.087	0.136	-0.406	-0.094	-0.212
FRP	0.674**	-0.073	0.701**	0.491	-0.080	0.496	0.163	0.081	-0.444	-0.136	-0.226
FC:N	-0.635**	0.203	-0.682**	-0.521*	0.054	-0.383	-0.075	-0.078	0.315	0.138	0.244
FC:P	-0.567*	-0.038	-0.710**	-0.476	0.183	-0.344	-0.191	0.035	0.348	0.239	0.255
FN:P	-0.118	-0.302	-0.231	-0.100	0.180	-0.093	-0.181	0.111	0.156	0.157	0.095
MC	0.631**	-0.283	0.294	0.484	0.310	0.465	-0.152	0.366	-0.192	0.242	-0.146
pH	0.457	-0.421	-0.017	0.208	0.362	0.454	-0.204	0.443	-0.194	0.349	0.047
BD	-0.586*	0.177	-0.321	-0.451	-0.229	-0.407	0.129	-0.301	0.174	-0.209	0.352
Sand	0.571*	-0.878**	-0.286	0.545*	0.781**	0.261	-0.670**	0.807**	0.243	0.766**	-0.215
Silt	-0.579*	0.878**	0.299	-0.562*	-0.800**	-0.256	0.694**	-0.819**	-0.270	-0.787**	0.235
Clay	-0.093	0.277	0.336	-0.058	-0.412	-0.081	0.290	-0.402	-0.061	-0.411	0.084
SOC	0.810**	-0.292	0.535*	0.581*	0.208	0.601*	-0.064	0.347	-0.376	0.146	-0.305
TN	0.228	0.314	0.278	-0.014	-0.145	0.355	0.210	-0.056	-0.379	-0.139	-0.070
TP	0.893**	-0.608*	0.215	0.770**	0.585*	0.532*	-0.432	0.682**	-0.074	0.521*	-0.355
C:N	0.803**	-0.700**	0.416	0.760**	0.403	0.401	-0.288	0.493	-0.101	0.315	-0.338
C:P	0.608*	-0.026	0.643**	0.348	-0.075	0.539*	0.187	0.066	-0.506*	-0.125	-0.225
N:P	-0.335	0.695**	0.113	-0.491	-0.494	0.005	0.452	-0.468	-0.300	-0.446	0.133
DOC	0.838**	-0.343	0.697**	0.555*	0.122	0.704**	0.084	0.255	-0.506*	0.055	-0.079
NH_4^+-N	-0.296	0.626**	0.562*	-0.222	-0.772**	-0.214	0.629**	-0.720**	-0.272	-0.771**	0.015
NO_3^--N	0.617*	0.042	0.725**	0.410	-0.143	0.491	0.223	0.011	-0.488	-0.202	-0.240
AP	0.879**	-0.762*	0.218	0.779**	0.614*	0.522*	-0.422	0.555*	-0.227	0.688*	-0.057
Fe	-0.597*	0.900**	0.220	-0.674**	-0.771**	-0.175	0.706**	-0.780**	-0.348	-0.721**	0.206
Al	0.606*	-0.208	0.087	0.523*	0.395	0.336	-0.337	0.473	-0.016	0.359	-0.438
MBC	0.958**	-0.631**	0.289	0.786**	0.561*	0.611*	-0.399	0.686**	-0.149	0.502*	-0.342
MBN	0.937**	-0.547*	0.496	0.798**	0.388	0.565*	-0.247	0.523*	-0.235	0.302	-0.387
MBP	0.938**	-0.517*	0.389	0.782**	0.462	0.580*	-0.319	0.588*	-0.187	0.397	-0.419
MBC:N	-0.142	-0.134	-0.751**	-0.194	0.436	-0.013	-0.430	0.384	0.347	0.541*	0.198
MBC:P	-0.902**	0.513*	-0.359	-0.822**	-0.485	-0.481	0.371	-0.584*	0.092	-0.414	0.534*
MBN:P	-0.875**	0.560*	-0.109	-0.771**	-0.641**	-0.491	0.526*	-0.727**	-0.024	-0.606*	0.473

Note: *, $0.01 < P \leq 0.05$, **, $P \leq 0.01$. H, Shannon-Wiener index; Lsc, litter layer standing crop; LOC, litter organic carbon; LTN, litter total nitrogen; LTP, litter total phosphorus; LC:N, litter organic carbon - total nitrogen ratio; LC:P, litter organic carbon - total phosphorus ratio; LN:P, litter total nitrogen - total phosphorus ratio; FRB, fine root biomass; FROC, fine root organic carbon; FRN, fine root nitrogen; FRP, fine root phosphorus; FC:N, fine root organic carbon - total nitrogen ratio; FC:P, fine root organic carbon - total phosphorus ratio; FN:P, fine root total nitrogen - total phosphorus ratio; MC, Moisture content; BD, bulk density; Sand, >0.02mm sand percentage; Silt, 0.002-0.02mm silt percentage; Clay, <0.002mm clay percentage; pH, soil pH value; SOC, soil organic carbon; TN, total nitrogen; TP, total phosphorus; C:N, soil organic carbon - total nitrogen ratio; C:P, soil organic carbon - total phosphorus ratio; N:P, soil total nitrogen - total phosphorus ratio; DOC, dissolved organic carbon; NH_4^+-N, ammonium nitrogen; NO_3^--N, nitrate nitrogen; AP, available phosphorus; Fe, total ferruml; Al, total aluminium; MBC, microbial biomass carbon; MBN, microbial biomass nitrogen; MBP, microbial biomass phosphorus; MBC:N, microbial biomass carbon - nitrogen ratio; MBC:P, microbial biomass carbon - phosphorus ratio; MBN:P, microbial biomass nitrogen - phosphorus ratio. BG, β-D-glucosidase; CBH, cellobiohydrolase; NAG, β-N-acetylglucosaminidase; ACP, acid phosphatase. $TER_{C:N}$, the threshold elemental ratios for C:N; $TER_{C:P}$, the threshold elemental ratios for C:P.

Figure 1S. Soil enzyme activity ratios at different vegetation restoration stages. PM, *Pinus massoniana* plantation; PL, *Pinus massoniana-Lithocarpus glaber* mixed broadleaved-conifer forest; CA, *Choerospondias axillaris* deciduous broadleaved forest; LG, *Lithocarpus glaber* evergreen broad-leaved forest; BG, β-D-glucosidase; CBH, cellobiohydrolase; NAG, β-N-acetylglucosaminidase; ACP, acid phosphatase. Different capital letters in the same column indicate significant differences ($p < 0.05$).

